

Additive Manufacturing of Polymer Matrix Composite Materials with Aligned or Organized Filler Material: A Review

Karl Niendorf and Bart Raeymaekers*

The ability to fabricate polymer matrix composite materials with continuous or discontinuous filler material, oriented in a user-specified direction, enables implementing designer material properties, such as anisotropic mechanical, thermal, and electrical properties. Conventional fabrication methods rely on a mold, which limits specimen geometry and is difficult to implement. In contrast, additive manufacturing, including fused filament fabrication or fused deposition modeling, direct ink writing, or stereolithography, combined with a method to align filler material such as a mechanical force or an electric, magnetic, shear force, or ultrasound wave field, enables 3D printing polymer matrix composite material specimens with complex geometry and aligned filler material, without the need for a mold. Herein, we review the combinations of fabrication and filler material alignment methods used to fabricate polymer matrix composite materials, in terms of operating and design parameters including size, resolution, print speed, filler material alignment time, polymer matrix and filler material requirements, and filler manipulation requirements. The operating envelope of each fabrication method is described and their advantages, disadvantages, and limitations are discussed. Finally, different combinations of 3D printing and filler material alignment methods in the context of important engineering applications, such as structural materials, flexible electronics, and shape-changing materials, are illustrated.

1. Introduction

Polymer matrix composite materials are multiphase materials that consist of a polymer matrix and a continuous or discontinuous filler material.^[1] It is well documented that the properties of polymer matrix composite materials depend on the properties of the matrix and filler material,^[2] the interface and dispersion of the filler material in the polymer matrix,^[3] and the spatial arrangement and alignment of the filler material in the polymer matrix.^[4] Changing the properties of the matrix material and the properties and/or arrangement of the filler material allows

designing and fabricating composite materials with potentially exotic characteristics,^[5] including advanced mechanical properties^[6,7] and anisotropic electrical^[8] and thermal^[9] conductivity. Such materials are of considerable interest to the scientific community because of their potential benefit to a myriad of engineering applications. Therefore, different categories of fabrication methods have been implemented.

Conventional fabrication methods of polymer matrix composite materials with continuous filler material produce high-quality, large-scale specimens, but typically involve several expensive production steps, including manufacturing a mold, impregnating fibers with polymer resin, autoclave curing, and/or postprocessing.^[10] On the other hand, conventional fabrication methods of polymer matrix composite materials with discontinuous filler material, such as mold casting^[11] and injection molding,^[12] rely on injecting a mixture of a liquid polymer matrix and filler material into a hollow cavity. These methods allow manufacturing a more intricate specimen geometry and are more economical than conventional methods used for composite materials with continuous

filler material because the mixture of a polymer and a discontinuous filler material can flow into tight spaces and corners and, additionally, automated mold processes quickly eject finished specimens before reusing the mold. However, they offer limited control of the spatial arrangement and alignment of the filler material and require a unique mold for each specimen geometry.

In contrast, additive manufacturing methods such as fused filament fabrication (FFF) or fused deposition modeling (FDM), direct ink writing (DIW), and stereolithography (SLA)^[13] enable fabricating complex specimen geometries without the need for a mold. They also create less waste than conventional fabrication methods^[14] and are largely automated, thus reducing both labor cost and human error. When combined with a method to spatially arrange or align/orient discontinuous filler material, we can use additive manufacturing methods to fabricate polymer matrix composite materials with designer properties and enable material designs that were previously impossible to manufacture. Thus, researchers have recognized the potential of such combined fabrication methods to control the spatial arrangement and alignment of the filler material in the context

K. Niendorf, Prof. B. Raeymaekers
Department of Mechanical Engineering
University of Utah
Salt Lake City, UT 84112, USA
E-mail: bart.raeymaekers@utah.edu

 The ORCID identification number(s) for the author(s) of this article can be found under <https://doi.org/10.1002/adem.202001002>.

DOI: 10.1002/adem.202001002

of manufacturing engineered materials. This is evidenced by a significant number of publications on various aspects of this topic in recent years, related to both additive manufacturing and methods to align the filler material in a polymer matrix. However, significant challenges remain, including dimensional scalability, repeatability, and limitations of material choice.^[15]

Thus, the objective of this article is to critically review the different combinations of additive manufacturing methods and filler material alignment techniques to fabricate engineered polymer matrix composite materials in a layer-by-layer fashion and compare their advantages and limitations to conventional fabrication methods.

2. Polymer Matrix Composite Material Fabrication and Filler Material Alignment Methods

2.1. Filler Material Alignment Methods

Filler materials vary in composition and length scale. Macroscale filler materials are typically fibrous and consist of continuous or chopped carbon, Kevlar, or glass fiber tow.^[16] Microscale filler materials^[17] include precisely chopped microfibers,^[18] micro-rods,^[19] and spherical^[20] and nonspherical^[21] particle powders. Nanoscale filler materials^[22] exist in more variations than macro- or microscale fillers, and include single-walled and multiwalled carbon nanotubes (SWCNTs and MWCNTs),^[23] carbon nanofibers (CNFs),^[24] graphene nanoplatelets (GNPs),^[25] and powders consisting of spherical particles.^[26]

Integrating a filler material into a polymer matrix occurs in three primary ways: 1) embedding continuous macroscale fiber tow in the polymer matrix,^[27] 2) spinning a liquid polymer or discontinuous nanofibers into a continuous fiber before embedding it in the polymer matrix, which has been accomplished using electrospinning,^[28] melt spinning,^[29] wet spinning,^[30] and direct spinning,^[31] and 3) directly dispersing discontinuous filler material into the polymer matrix.^[32] The first two methods rely on the geometry of the continuous fiber and mechanical (tension) forces to orient it in the desired direction, for instance, through rollers within an extrusion nozzle of an FDM or FFF printer, whereas the third method results in randomly oriented dispersed filler material in the polymer matrix.

The properties of the polymer matrix composite material depend on the spatial arrangement and the alignment of the filler material within the polymer matrix. For instance, it is well known that aligning micro- and nanoscale filler material in the direction of mechanical loading improves its mechanical properties by providing reinforcement^[33] and enhances its electrical^[34] and thermal^[35] conductivity by reducing the percolation threshold in the alignment direction.^[36,37]

Several methods exist to spatially arrange and/or align discontinuous filler material in the polymer matrix. Electric^[38] and magnetic^[39] fields orient the filler material in the field direction but require ultrahigh field strengths (of the order of 20 kV m^{-1} ^[40] and 8000 mT ,^[41] respectively), thus limiting dimensional scalability of the specimens. In addition, the filler material must be electrically conductive or ferromagnetic, respectively, which limits material choice. A shear force field creates flow (liquid specimen)^[42] or strain (solid specimen)^[43] to orient the filler material,

typically in the direction of the shear force. Ultrasound wave fields spatially arrange^[44] and orient^[45] the filler material by means of the acoustic radiation force associated with the ultrasound wave, independent of its material properties or shape.^[46] Further, ultrasound wave fields exhibit low attenuation in low-viscosity fluids,^[47] thus facilitating dimensional scalability.

2.2. Methods to Quantify the Filler Material Alignment and Orientation

Several methods exist to quantify the filler material alignment in a composite material specimen. Raman spectroscopy compares the intensity of Raman spectra between specimens with different filler material alignments.^[48] However, Raman spectroscopy requires specialized equipment and does not quantify the primary filler material alignment angle. Also, it does not provide information about individual filler material particles, but only of the material specimen as a whole. A different method uses digital image processing to calculate a fiber orientation factor, which quantifies the difference between the primary filler material orientation angle and a specified axis.^[49,50] However, individual filler material particles must be selected by hand, which may introduce human bias or error. Alternatively, measuring filler material alignment anisotropy using a fast Fourier transform (FFT) yields information about the distribution of the alignment angles of individual filler material particles.^[51] This method does not require specialized equipment or human intervention.

2.3. Polymer Matrix Composite Material Fabrication Methods

2.3.1. Mold Casting

Figure 1 shows a schematic of a typical mold casting setup, which involves injecting a mixture of a liquid polymer resin and a discontinuous filler material into a 3D mold cavity that is often made from metal, glass, or a rigid polymer. The polymer resin and filler material mixture conforms to the 3D mold cavity to give the specimen its shape (**Figure 1a**), and external field transducers (shown in red) create a force that aligns the filler material, dispersed in the polymer resin, into a user-specified orientation and location, thus controlling the microstructure of the material specimen (**Figure 1b**). The liquid polymer resin hardens or cures, driven by external stimuli or an internal chemical reaction, fixating the aligned filler material in the polymer matrix, before evacuating the solid specimen from the mold cavity (**Figure 1c**). We use mold casting as a benchmark to which we compare the different additive manufacturing techniques that are the subject of this review. The additive manufacturing methods we include in this review categorize into either extrusion or SLA methods.

2.3.2. Extrusion Fabrication Methods

Extrusion methods selectively deposit a liquid polymer with a continuous or dispersed filler material through a nozzle to form a 3D geometry with distinct layers.^[13] **Figure 2** shows a typical FFF setup that uses a polymer matrix with continuous filler material. Spools supply filament wires of the continuous filler material (black) and polymer matrix (yellow) into a heated extruder

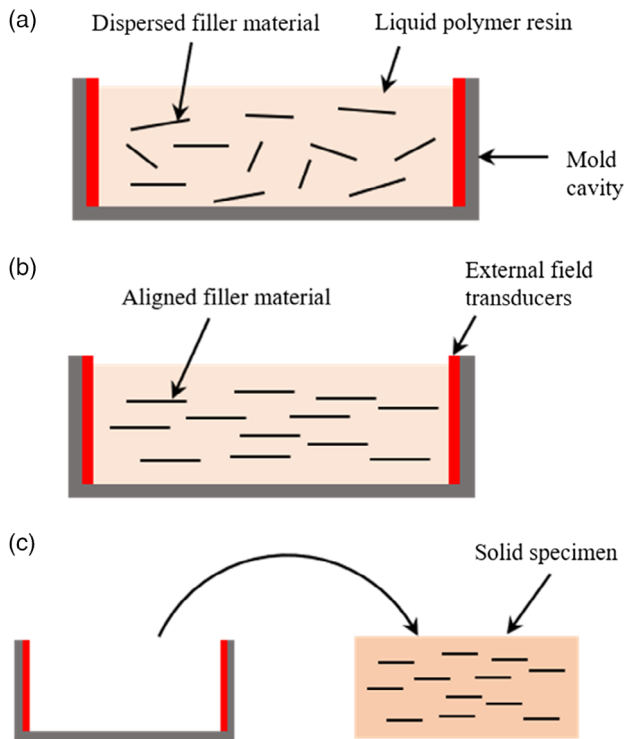


Figure 1. Schematic of a typical mold casting setup in which a) a mixture of liquid polymer resin and dispersed filler material is injected into a 3D mold cavity, b) an external field aligns the filler material, and c) the polymer resin cures and the solid specimen is evacuated from the mold cavity.

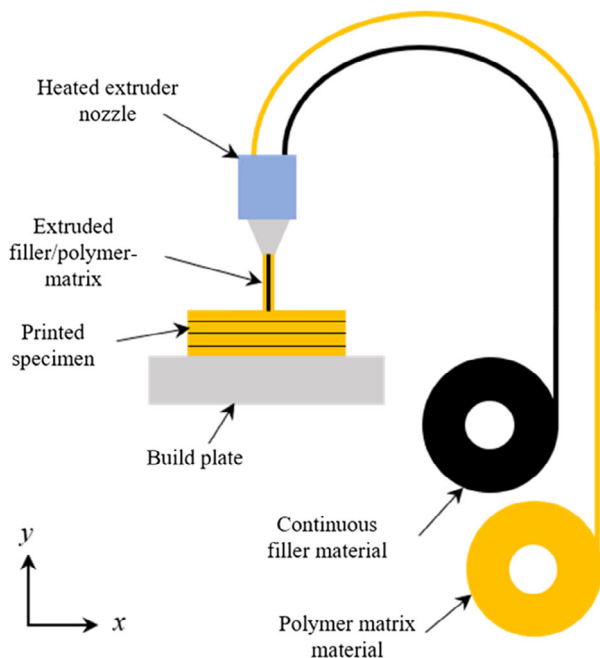


Figure 2. Schematic of a typical FFF setup with spools of continuous filler material (black) and polymer matrix (yellow) filament material. The filament feeds into a heated extruder nozzle and selectively deposits on a build plate to print a 3D specimen in a layer-by-layer fashion.

nozzle that melts the polymer matrix material, which surrounds the continuous filler material as it exits the nozzle and deposits on the build plate. Thus, this method fabricates a 3D specimen geometry by controlling the position of either the extruder nozzle or build plate to selectively deposit filler material and polymer matrix material in a layer-by-layer fashion.

2.3.3. SLA Fabrication Methods

SLA additive manufacturing methods rely on selectively projecting UV light into a vat of photocurable polymer resin to polymerize a 2D geometry. **Figure 3** shows a schematic of a typical a) laser and b) digital light processing (DLP) projection SLA setup. In both setups, a photopolymer resin is mixed with a discontinuous filler material and injected into a resin vat. External field transducers (shown in red) align the filler material before a UV light source selectively cures a 2D layer of the photopolymer resin. The cured layer of photopolymer resin adheres to a computer-controlled build plate that enables fabrication of a 3D specimen in a layer-by-layer fashion.

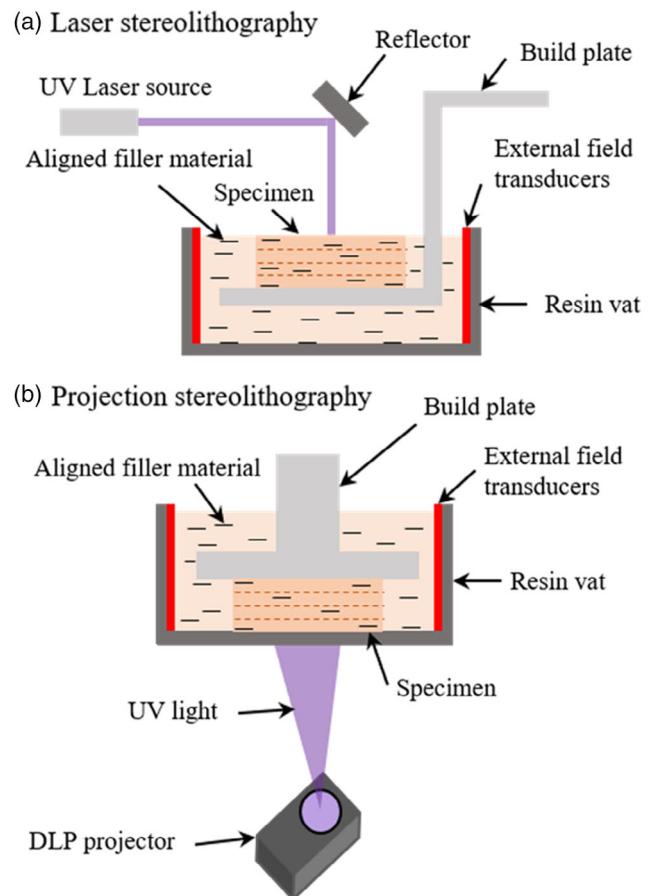


Figure 3. Schematic of a typical a) laser and b) DLP projection SLA additive manufacturing setup. External field transducers (red) align the filler material (black) into a user-specified orientation and UV light cures a 3D specimen in a layer-by-layer fashion.

2.4. Combining Additive Manufacturing and Filler Material Alignment Methods

Fabricating polymer matrix composite materials with aligned or spatially organized filler material requires combining a fabrication method with a method to align and/or spatially arrange the filler material. We used combinations of keywords to search the literature, including additive manufacturing, nanocomposite and microcomposite materials, fused filament fabrication, fused deposition modeling, direct ink writing, stereolithography, directed self-assembly, aligned filler material, AC/DC electric, magnetic, shear force and ultrasound wave field alignment, and found 99 journal articles in the open literature that are relevant to this review. **Figure 4** shows the number of journal articles as a function of publication year, with colors indicating different fabrication methods (Figure 4a) and filler material alignment methods (Figure 4b), respectively. We note increasing interest in this topic since the mid-2010s.

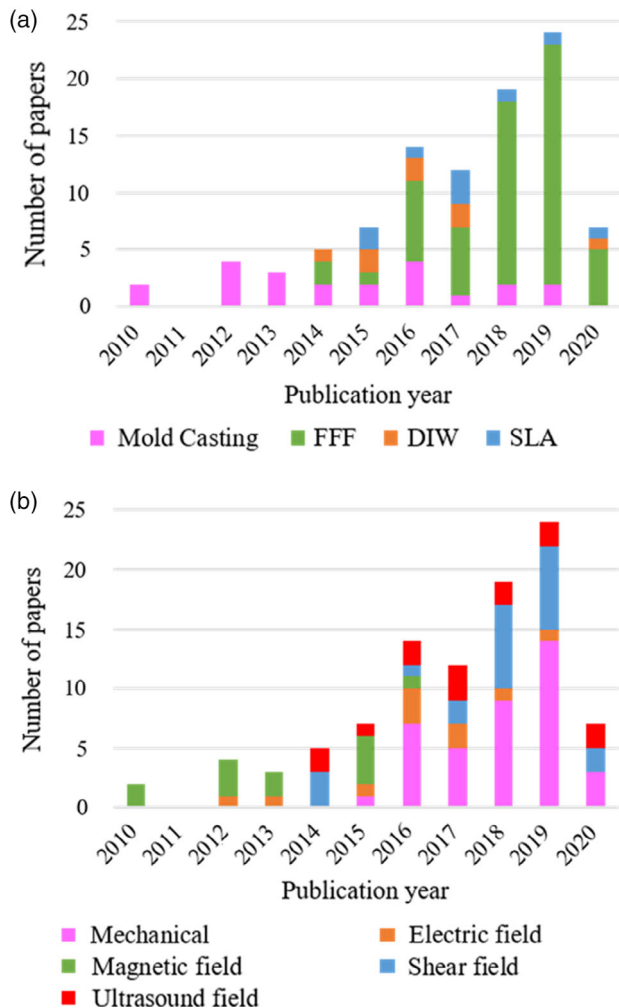


Figure 4. Number of journal publications published in the open literature as a function of publication year, organized by a) fabrication method and b) filler material alignment method, to fabricate polymer matrix composite materials with aligned filler material.

3. Review and Discussion of Combined Fabrication and Filler Material Alignment Methods

The literature documents various combinations of polymer matrix composite material fabrication and filler material alignment methods. In this section, we methodically review the state of the art and discuss advantages and disadvantages of each combination of methods.

3.1. Mold Casting Fabrication

Mold casting is a conventional fabrication method that relies on a liquid polymer flowing into a 3D mold cavity before solidifying in its shape. Because the setup is simple compared to other fabrication methods discussed further in this article, the mold casting process combines with a wide variety of polymer resins, filler materials, and filler material alignment methods, which renders it appropriate for many different engineering applications. Polymer matrix materials that work well with mold casting display low viscosity at room temperature to facilitate material flow in the mold, and filler material dispersion and alignment in the matrix material. Thus, polymer matrix materials used with mold casting include epoxy resin,^[52] polyvinylidene fluoride,^[34] urethane,^[49] and polycarbonate.^[39] The length scale of filler materials varies from nanoscale to microscale and any material limitations relate to the filler material alignment method. As such, the literature documents that polymer matrix composite materials have been fabricated using mold casting in combination with external AC electric,^[53] DC electric,^[8] magnetic,^[54] and ultrasound wave^[33] fields to organize and align the filler material.

3.1.1. Mold Casting Combined with an Electric Field

Khan et al. used DC electric fields of 10–20 V mm⁻¹ to align up to 0.5 wt% MWCNTs in an epoxy matrix within a glass mold (see schematic of experimental setup in **Figure 5a** and material specimen in **Figure 5b**).^[8] They used UV light and ozone treatment to modify the MWCNT surface from hydrophobic to hydrophilic, which improves MWCNT dispersion^[55] and adhesion to the matrix material. They found that the electrical conductivity increases with increasing MWCNT weight percent, parallel to the alignment direction. Instead of a DC electric field, Ladani et al. combined mold casting with an AC electric field of 30 V mm⁻¹ (10 kHz operating frequency, 1 h exposure time) to align up to 1.6 wt% CNFs (135 nm diameter, 20 μm length) in an epoxy matrix, within a 2 mm thick rectangular cavity formed between two carbon fiber/epoxy prepreg strips that also act as electrodes.^[56] Although the composite material specimens were limited by the mold geometry and the time to align the CNFs, they showed that the electrical conductivity increased with increasing CNF weight percent and CNF alignment by lowering the percolation threshold compared to composite materials with randomly oriented CNFs. Alignment is particularly important for small compared to large CNF weight percent because it is increasingly difficult to obtain a percolated network of CNFs with decreasing weight percent. Similarly, Wu et al. used an AC electric field of 30 V mm⁻¹ (10 kHz operating frequency,

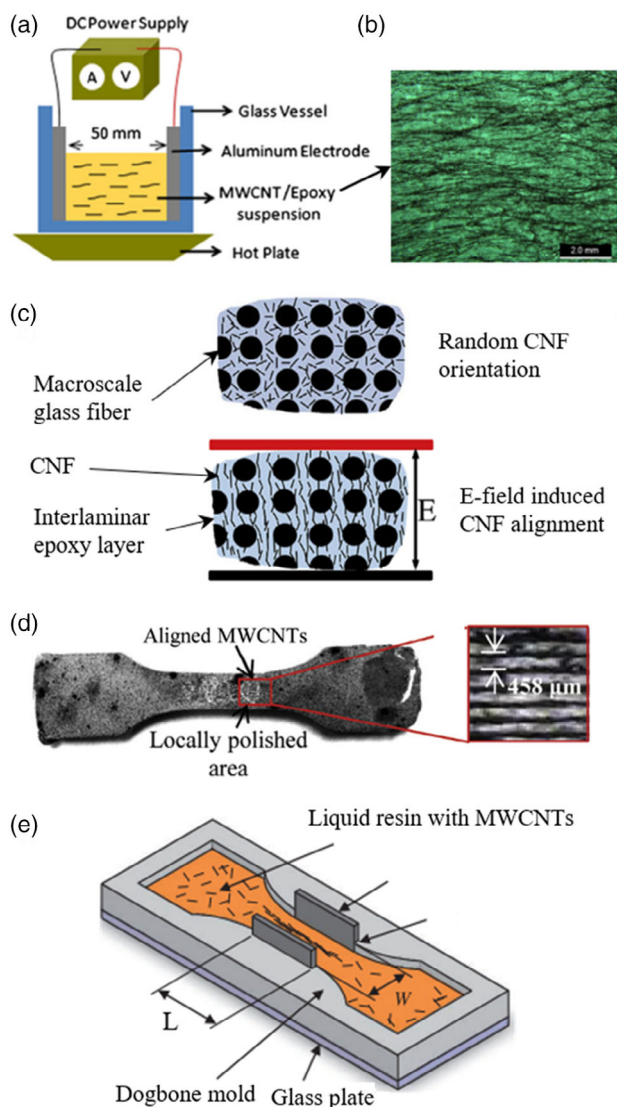


Figure 5. a) Schematic of a rectangular mold used to cast electrically aligned MWCNT/epoxy composite materials. Reproduced (adapted) with permission.^[8] Copyright 2013, Elsevier. b) Specimen fabricated using the setup of (a). c) Schematic of CNFs electrically aligned in the interlaminar layer of a macroscale glass-fabric composite material (modified from Wu et al. Modified and reproduced (adapted) with permission.^[57] Copyright 2017, Elsevier. d) MWCNTs embedded in a dogbone-shaped polymer matrix composite material, aligned using an ultrasound wave field. The locally polished area reveals the aligned MWCNTs. Reproduced (adapted) with permission.^[49] Copyright 2014, Elsevier. e) Schematic of a dogbone-shaped mold used to mold cast urethane-matrix composite materials with greater than 10 wt% of MWCNTs aligned using an ultrasound wave field. Modified and reproduced (adapted) with permission.^[33] Copyright 2018, Sage Journals.

24 h exposure time) to align CNFs (100 nm diameter, 125 μm length) in an epoxy matrix under vacuum, but they created a hybrid macro- and nanoscale 170 mm \times 20 mm \times 7 mm composite material specimen in which the aligned CNFs and epoxy mixture formed an interlaminar matrix between layers of macroscale glass fibers (see Figure 5c).^[57] Both the mold geometry and interlaminar spacing limited the size and complexity of the

material specimen. Pothnis et al. also used mold casting, but with a nonuniform rather than uniform AC electric field (up to 27 V mm^{-1} , 15 min exposure time), to align up to 0.1 wt% MWCNTs (12.5 nm diameter, 5.5 μm length) in epoxy.^[53] Their fabrication method relied on dielectrophoresis (DEP), which is the force that a nonuniform electric field exerts on a dielectric particle.^[58] They fabricated 60 mm \times 50 mm \times 3 mm tensile test specimens and found that the nonuniform field reduced the voltage required to align electrically conductive filler material by as much as 80% compared to a uniform AC electric field, which aided the dimensional scalability of electric field-based filler material alignment methods and resulted in an electrode separation distance 7.57 times larger than the one used in reference.^[57]

3.1.2. Mold Casting Combined with a Magnetic Field

Erb et al. combined mold casting with an external magnetic field to fabricate multilayer hydrogel materials with aligned aluminum oxide platelets (7.5 μm diameter, 200 nm thick).^[59] They first coated the aluminum oxide platelets with iron-oxide nanoparticles to make them ferromagnetic and then organized them into different bioinspired patterns within the hydrogel matrix by rotating a rare-earth magnet above the Teflon mold. They obtained a 3D geometry by stacking multiple mold cast layers, which then self-shaped into programmed configurations with controlled hydration or drying of the hydrogel matrix.

3.1.3. Mold Casting Combined with an Ultrasound Wave Field

Scholz et al. used an ultrasound wave field within a 30 mm \times 15 mm rectangular mold to align up to 9 vol% of glass microfibers (14 μm diameter, 50 μm length) in several polymer resin materials, including epoxy, polyester, silicon, and agar, and estimated that their setup produced a maximum pressure (ultrasound) wave of 1.2 MPa (80 V_{pp}, 2.01 MHz operating frequency) without inducing streaming or boiling in the polymer resin.^[60] They reported that the glass fiber alignment increased the material specimen strength by 43% in the direction of mechanical loading. These results are similar to those documented by Haslam et al., who used an ultrasound wave field (1.477 MHz operating frequency) to align MWCNTs (65 nm average diameter, 15 μm average length) in a polymer matrix to manufacture 68 mm \times 7.5 mm \times 5 mm nanocomposite specimens (see Figure 5d).^[49] Greenhall et al. also used an ultrasound wave field (190 kHz operating frequency) in the gauge section of a dogbone-shaped acrylic mold to fabricate macroscale urethane-matrix specimens with over 10 wt% of aligned MWCNTs (65 nm average diameter, 15 μm average length) (see Figure 5e).^[33] To accomplish this ultrahigh weight percent, they first dispersed 1.0 wt% of MWCNTs in the matrix material and used acoustic focusing to align the MWCNTs into a single line before they removed excess matrix material where MWCNTs no longer existed after acoustic focusing (or existed at a much lower concentration). This process circumvents problems of high viscosity and dispersion caused by adding a large weight percent of filler material in the polymer matrix. They showed that the ultrahigh weight percent of MWCNTs increased the ultimate tensile strength of the polymer matrix composite material by \approx 73% compared to the virgin matrix.

3.2. Extrusion-Based Fabrication Methods

3.2.1. Fused Filament Fabrication

Fused filament fabrication, which is equivalent to Stratasys's trademarked term "fused deposition modeling,"^[61] is an additive manufacturing technology that uses a computer-controlled extruder nozzle to heat, melt, extrude, and selectively deposit a polymer filament on a build plate, into a user-specified 3D geometry.^[13] FFF relies on solid polymer filament melting and resolidifying,^[62] thus limiting filament materials to thermoplastics such as acrylonitrile butadiene styrene (ABS),^[63] polyamide (PA) or nylon,^[64] polylactic acid (PLA),^[65] and polypropylene (PP).^[66] The filler material for FFF-printed polymer matrix composite materials frequently consists of continuous carbon,^[67] glass,^[68] or Kevlar^[69] tow, but also includes discontinuous filler material such as short chopped carbon fibers^[70] and CNFs.^[71]

FFF Using Filament with Pre-embedded Filler Material: Discontinuous filler material can be embedded into a thermoplastic filament prior to extrusion and deposition in an existing FFF printer.^[72] (see Figure 6a). FFF methods that incorporate discontinuous filler material in the filament rely on shear forces in the converging extruder nozzle geometry to align the filler material as it deposits and resolidifies on a build plate.^[73] Ferreira et al. used FFF to print PLA composite materials with aligned carbon microfibers (1.75 mm filament diameter, 60 μm microfiber length).^[74] They printed 165 mm \times 19 mm \times 3.3 mm dog-bone and 200 mm \times 25 mm \times 4.8 mm rectangular composite material specimens for tensile and shear testing, respectively, with 0°, 90°, and $\pm 45^\circ$ layer orientations, 50 mm s⁻¹ print speed, and a 100% rectilinear infill. They compared virgin PLA composite materials to those with 15 wt% carbon microfibers and concluded that the addition of microfibers increases the specimen stiffness by 220% in the printing direction. In another study, Mulholland et al. used an FFF printer with a commercially available Onyx filament (1.75 mm diameter)^[75] to 3D print air-cooled heat exchangers with anisotropic thermal conductivity using PA with 14.1 wt% chopped carbon fibers (10 μm diameter), and with a 50 mm s⁻¹ print speed, 0.35 mm extruder nozzle diameter, and 0.1 mm layer thickness.^[73] They quantified carbon fiber alignment according to the tensor approach proposed by Advani and Tucker^[76] and found that the fibers aligned with the shear direction (a_{11}), such that average tensor alignment components were $a_{11} = 0.81$, $a_{22} = 0.08$, and $a_{33} = 0.11$, where perfect alignment required $a_{11} = 1$ and $a_{22} = a_{33} = 0$. Spoerk et al. also confirmed filler material alignment resulting from a shear force field. They used an FFF printer to fabricate 80 mm \times 10 mm \times 4 mm PP composite material specimens with chopped carbon microfibers (7 μm diameter, 250 μm length) and reported 200% greater thermal conductivity in the alignment direction than the virgin PP.^[66]

FFF with Separate Extruder Nozzles for Matrix and Continuous Filler Materials: Rollers or an extruder nozzle can mechanically align and embed continuous filler material directly in the specimen during printing. This method requires two separate extruder nozzles (see Figure 6b)—one for the filler material and one for the matrix material—thus allowing aligning and embedding the filler material across an entire specimen layer or selectively in specific locations.^[77] The MarkForged Mark One^[78] uses a dual extruder nozzle system and is the first desktop

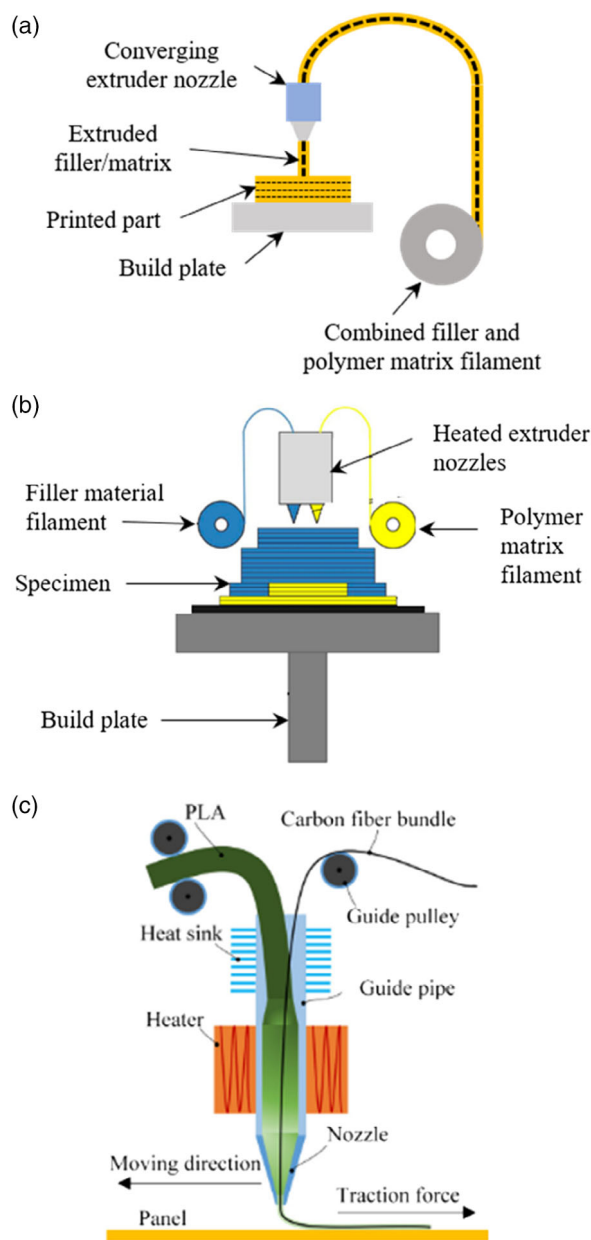


Figure 6. a) FFF printer with filament comprising discontinuous filler material preembedded in a polymer matrix. b) FFF printer with separate extruder nozzles to selectively deposit filler material and polymer matrix filament. Modified and reproduced (adapted) with permission.^[77] Copyright 2017, Taylor and Francis, <https://www.tandfonline.com/>. c) FFF printer with a single extruder nozzle to mix filler and polymer matrix material and deposit the mixture simultaneously. Reproduced (adapted) with permission.^[86] Copyright 2016, Elsevier.

FFF printer capable of fabricating polymer composite material specimens with continuous fiber filler material. Justo et al. used a Mark One to fabricate 310 mm \times 90 mm PA composite material specimens with continuous carbon or glass fiber filler material and reported that the filler material improved the mechanical properties compared to virgin PA, but the strength of specimens was not comparable to that of composite materials fabricated

with conventional methods.^[68] MarkForged released the Mark Two in 2016,^[79] which is capable of a 280 mm s^{-1} print speed and $100 \mu\text{m}$ layer resolution, compared to 200 mm s^{-1} and $200 \mu\text{m}$, respectively, for the Mark One. Caminero et al. used a Mark Two to print $80 \text{ mm} \times 10 \text{ mm} \times 4 \text{ mm}$ PA (1.75 mm diameter filament) matrix composite material specimens with continuous carbon, glass, and Kevlar fiber bundles (0.33, 0.30, 0.30 mm diameter, respectively) with a 100% density rectangular infill pattern.^[80] They documented a 386%, 777%, and 1233% impact resistance increase of PA composite materials with continuous carbon, glass, and Kevlar filler material, respectively, compared to virgin printed materials. Pyl et al. also used the Mark Two to fabricate $200 \text{ mm} \times 30 \text{ mm} \times 1.25\text{--}1.625 \text{ mm}$ rectangular and $165 \text{ mm} \times 36 \text{ mm} \times 2.25 \text{ mm}$ dumbbell PA matrix composite material specimens, respectively, with aligned continuous carbon fibers.^[81] They found that drilling holes, with continuous filler material placed concentrically around the drilling location, reduces stress concentrations compared to printing holes. In a different study, Naranjo-Lozada et al. used the Mark Two to print three types of $57 \text{ mm} \times 13 \text{ mm} \times 3.2 \text{ mm}$ tensile test specimens: PA (1.75 mm filament diameter), Onyx (1.75 mm filament diameter), and PA with continuous carbon fiber (0.35 mm tow diameter) filaments with 4–54 vol% filler material.^[82] They reported that printing with a triangular rather than rectangular infill pattern displayed the highest tensile strength, but that the infill density affected tensile properties in a minor fashion only, such that a 85.7% reduction in infill density yielded a 7.4% and 30.4% reduction of the tensile strength and printing time, respectively, for rectangular Onyx specimens. Further, Chabaud et al. also used the Mark Two to print $100 \text{ mm} \times 15 \text{ mm} \times 0.5\text{--}2 \text{ mm}$ PA matrix tensile test specimens with aligned continuous carbon or glass fibers (6.9 μm average carbon fiber diameter, 8.8 μm average glass fiber diameter), 14 mm s^{-1} print speed, and 100–200 μm layer thicknesses. They reported that the continuous fiber radius (0.62 mm for carbon fiber and 0.66 mm for glass fiber) that formed when the extruder nozzle changed direction when printing parallel lines of filler material, for example, at the boundaries of the specimen, created stress concentrations, and even caused local fiber breakage in the carbon filaments due to low toughness.^[83]

FFF with a Single Extruder Nozzle and Separate Spools of Matrix and Continuous Filler Materials: The filler material and polymer matrix material can mix in the extruder nozzle and deposit on the build plate simultaneously^[84] (see Figure 6c). Hou et al. used an FFF setup that combined separate filament spools of continuous Kevlar fibers (density $\rho = 1440 \text{ kg m}^{-3}$) and PLA resin (1.75 mm diameter) in a single extruder nozzle to fabricate $60 \text{ mm} \times 60 \text{ mm} \times 15 \text{ mm}$ composite material sandwich structures.^[85] They studied the effect of printing process parameters, including layer thickness (0.1–0.5 mm), cell length (9–13 mm), and filler material volume percent (2–11.5%), on the mechanical properties of the resulting specimens. They found that the maximum compression strength of the resulting composite material increased with increasing filler material volume percent, with a maximum of 17.17 MPa for 11.5 vol%. Similarly, Li et al. developed an FFF printer that simultaneously extruded PLA using a screw extruder and a continuous carbon fiber (bundle of 1000 fibers) filler material (see Figure 6c).^[86] They designed the extruder nozzle with a heat sink at the inlet, using solid-state

PLA, a conical nozzle to uniformly mix the carbon fiber and PLA, and a circular extruder nozzle outlet to ensure constant friction force of the PLA/carbon fiber strand under any print angle. They printed $110 \text{ mm} \times 27 \text{ mm} \times 2.3 \text{ mm}$ and $55 \text{ mm} \times 12 \text{ mm} \times 2.3 \text{ mm}$ rectangular composite material specimens and studied the effect of pretreating the continuous carbon fiber tow with a PLA sizing agent, to enhance PLA resin infiltration in the carbon fiber tow and interfacial adhesion during printing, and they found that the surface-modified carbon fiber filler material increased the tensile strength and flexural strength of the composite material specimens by 13.8% and 164%, respectively, compared to using non-surface-modified carbon fiber filler material. Heidari-Rarani et al. also designed an extruder nozzle that simultaneously extruded PLA (1.75 mm diameter) and continuous carbon fiber (7 μm diameter), which could attach to commercially available FFF printers. They printed $250 \text{ mm} \times 15 \text{ mm} \times 3.2 \text{ mm}$ rectangular PLA composite material specimens with 28.2 vol% carbon fiber, a 20 mm s^{-1} print speed, and a 300 μm layer thickness.^[87] They reported that a minimum distance of 0.4–0.5 mm should be maintained between adjacent print lines to avoid carbon fiber breakage in the radii at the ends of a specimen.

3.2.2. Direct Ink Writing

Direct ink writing, also known as “field-assisted deposition,” is an additive manufacturing process in which a liquid polymer matrix composite ink selectively extrudes, deposits, and cures to form a 3D material specimen.^[13] Unlike FFF techniques, which require melting of a thermoplastic filament, DIW extrudes material from liquid ink reservoirs, thus allowing inks to consist of colloids, thermosets, nanoparticles, and/or organic materials.^[88] Ideal DIW ink materials exhibit shear thinning to facilitate flow through the extruder nozzle, but are otherwise viscous for shape retention after deposition.^[89,90] A few researchers have demonstrated integrating DIW with external fields to align filler material dispersed in the liquid ink. Print speeds are typically below 10 mm s^{-1} ^[91,92] but can be as fast as 20 mm s^{-1} .^[93]

DIW Combined with a Shear Force Field: Compton and Lewis fabricated 3D printed cellular composite materials using an epoxy ink with multiple shear-aligned filler materials for enhanced mechanical performance.^[94] They modified the ink rheology to impart shear thinning by adding nanoclay platelets (1 nm thick, 100 nm length), silicon carbide whiskers (0.65 μm diameter, 12 μm length), and carbon microfibers (10 μm diameter, 220 μm mean length) for structural support. Then, they used a DIW printer to fabricate materials with hierarchical geometric patterns inspired by balsa wood, with a cell wall thickness ranging between 200 and 350 μm and specimen dimensions ranging between 88 and 20 mm. **Figure 7** shows a) a rendering of the setup and b) an optical image of a 3D printed honeycomb structure, with c,d) inset images showing the carbon microfiber and silicon carbide whisker alignment resulting from a shear and flow field. Gladman et al. also fabricated $57.5 \text{ mm} \times 30 \text{ mm}$ polymer matrix composite structures inspired by natural materials with DIW.^[95] They printed hydrogel filaments (600 μm diameter) with shear-aligned cellulose fibers that mimic plant cell walls (see Figure 7e). The materials exhibited anisotropic stiffness and

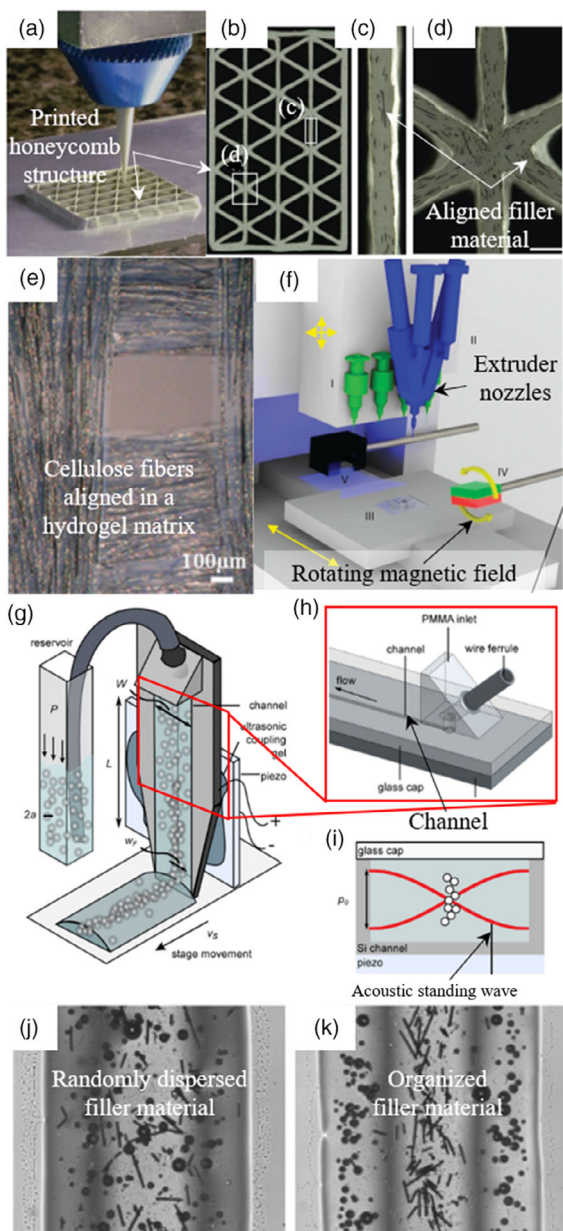


Figure 7. a) Rendering and b) optical image of a triangular honeycomb composite material specimen printed using DIW assisted by a shear force field. Modified and reproduced (adapted) with permission.^[94] Copyright 2014, Wiley. c) and d) show magnified optical images of b) Modified and reproduced (adapted) with permission.^[94] Copyright 2014, Wiley. e) Hydrogel filaments with shear force-aligned cellulose filler material. Reproduced (adapted) with permission.^[96] Copyright 2017, Springer Nature. f) DIW with multiple extruder nozzles and a rotating magnetic field to align filler material in polyurethane matrix material. Modified and reproduced (adapted) with permission.^[97] Copyright 2015, Springer Nature. g) Schematic of DIW setup with piezoelectric transducer, with h) inset image of extruder nozzle inlet and channel, to establish i) a standing ultrasound wave across the extruder nozzle channel. Modified and reproduced (adapted) with permission.^[93] Copyright 2017, Elsevier. j) Randomly dispersed silicon carbide microfibers and hollow glass spheres that k) organize into distinct and separate lines when exposed to an external standing ultrasound wave field. Modified and reproduced (adapted) with permission.^[91] Copyright 2016, Elsevier.

swell in response to external stimuli, enabling designing and 3D printing of complex shape-changing materials. Further, Lewicki et al. used shear force fields with DIW to align carbon microfibers (6 μm diameter, 300 μm length) in a thermoset resin and reported that both silica nanoparticles and carbon microfibers enhance shear thinning of the resin, which is important in light of extruding the material consistently, and also avoiding clogging of the extruder nozzle.^[96]

DIW Combined with a Magnetic Field: Kokkinis et al. used the magnetic field of a neodymium magnet during DIW to align 1 wt% alumina platelets, modified with iron-oxide nanoparticles to render them ferromagnetic, in 15 mm \times 15 mm \times 15 mm polyurethane specimens.^[97] Multiple extruder nozzles that enabled using multiple ink formulations in the same print deposited ink on a build platform before the platform moved below a rotating magnetic field (40 mT, 500 rpm) to orient the platelets in a user-specified direction (see Figure 7f).

DIW Combined with an Ultrasound Wave Field: Friedrich et al. used DIW in tandem with an ultrasound wave field (2.09 MHz operating frequency) to print 350–750 μm wide composite material specimens comprising an epoxy matrix with aligned glass microspheres (14–31 μm diameter).^[93] Figure 7g shows a schematic of the setup, in which they used a piezoelectric ultrasound transducer (10 mm \times 10 mm \times 1 mm) to establish a standing ultrasound wave across the extruder nozzle and channel (see Figure 7h). The standing ultrasound wave defines a low-pressure region at its nodes, which coincides with the center of the channel in Friedrich's work (see Figure 7i). Although accommodating ultrasound transducers complicates the extruder nozzle design compared to methods that use shear force field alignment, the low-pressure regions of the standing ultrasound wave allow control over the alignment and arrangement of filler material. Friedrich et al. studied the effect of printing parameters (filler material volume percent [1.7–9], ultrasound transducer input voltage [0–50 V_{pp}], print speed [1–20 mm s^{-1}]), including ink properties (fumed silica content [5–10 wt%], acetone content [8–24 wt%]), and ultrasound wave field parameters on the spatial distribution of the filler material and ink shape retention, and found that the ultrasound transducer input voltage had the strongest effect on filler material distribution because it corresponds to the pressure amplitude of the ultrasound wave field. Further, Collino et al. used DIW (350 μm wide extruder nozzle) with an ultrasound wave field (2.04–3.32 MHz operating frequency) to fabricate epoxy filament (up to 25 mm long) with different filler materials (7–34.5 μm diameter, 0.5–11.8 wt% per filler material) and demonstrated selectively organizing filler materials along different lines according to their material properties.^[91] Figure 7j shows randomly dispersed silicon carbide microfibers (7 μm diameter, 26–63 μm length) and hollow glass spheres (31 μm outer diameter) that are organized into distinct and separate lines of discontinuous filler material according to their density and compressibility, respectively, and located at the nodes or antinodes of a standing ultrasound wave field (Figure 7k). Wadsworth et al. fabricated 80 mm \times 10 mm \times 1 mm composite material specimens comprising a photopolymer and lines of aligned nickel-coated carbon microfibers (10 μm diameter, 100 μm length) by combining DIW with 2.15–6.35 mm s^{-1} print speeds and an ultrasound wave field of different operating frequencies (1.0–2.0 MHz).^[92] They used a standard FFF

printer with a modified extruder nozzle that incorporated two parallel-mounted ultrasound transducers to align the carbon microfibers as the filament deposits on the build plate. Using this fabrication method, they documented macro- and microscale alignment of the microfibers, evidenced by optical imaging and electrical conductivity measurements.

3.3. SLA Fabrication Methods

SLA is an additive manufacturing process that relies on a computer-controlled laser^[98] or a UV light projector^[99] to selectively cure photosensitive thermosetting resin in a layer-by-layer process to fabricate a 3D material specimen.^[100] Both controlled UV light exposure and specific photopolymer chemistry are essential to ensure that photopolymer cross-linking occurs only in desired locations.

3.3.1. Laser-Based SLA Combined with an External Field

Llewellyn-Jones et al. fabricated single-layer, 20 mm × 2 mm × 1 mm arbitrary-shaped photopolymer composite material specimens with aligned glass microfibers (14 μm diameter, 50 μm length) using a laser-based SLA method and an ultrasound wave field (see **Figure 8a**).^[101] They used parallel-oriented ultrasound transducers (2.35 MHz operating frequency, 60 V_{pp}) to align glass fibers dispersed in photopolymer resin into evenly spaced (≈300 μm) lines (see **Figure 8b**) and then selectively cured the photopolymer using a motion-controlled laser beam. They reported difficulty controlling layer thickness and printing multilayer specimens because their setup does not include a build plate to control the thickness and location of the printed specimen.

3.3.2. Projection-Based SLA Combined with an External Field

In contrast to laser-based SLA methods, which trace the photopolymer areas to cure, UV light projection SLA methods cure a single material layer at once, which increases the fabrication speed. Martin et al. presented a projection-based SLA method with a rotating magnetic field^[54] to orient 15 vol% iron-oxide-coated ceramic microplatelets (7.5 μm diameter, 350 nm thickness) into 90 μm architectures.^[21] They sequentially and selectively cured photopolymer resin layers and changed the magnetic field orientation using electromagnetic solenoids (114 mm inner diameter, 152 mm outer diameter, 21 mm thickness), located below and to the sides of the photopolymer reservoir, until the desired filler material architecture (22 mm × 22 mm × 3 mm) was complete (see **Figure 8c**). Yang et al. also used a projection-based SLA method with a DC electric field (30 V mm⁻¹), produced by parallel plate electrodes on a rotating stage, to align surface-modified MWCNTs in a photopolymer resin into bioinspired architectures.^[102] They printed composite material specimens with up to 90 layers (2.4 mm × 2.4 mm × 50 μm layers, ≈25 s layer⁻¹) with varying alignment angles of the MWCNTs (see **Figure 8d**), and they demonstrated that the compressive material properties of the printed composite material specimens increased with decreasing alignment angle increment between adjacent material layers.

Greenhall and Raeymaekers combined projection-based SLA and an ultrasound wave field within an octagonal acrylic reservoir with four sets of parallel-oriented ultrasound transducers (1.65 MHz operating frequency, 25 V_{pp}), (see **Figure 8e**) to 3D print 8.0 mm × 5.0 mm × 1.8 mm multilayer composite material specimens with aligned nickel-coated carbon microfibers (10 μm diameter, 100 μm length).^[103] They reported that the lines of aligned microfibers formed a percolated network that created anisotropic electrical conductivity in the material (average resistance of 59.7 Ω in the alignment direction and 112.7 MΩ perpendicular to alignment). Subsequently, Niendorf and Raeymaekers used Greenhall and Raeymaekers's fabrication method to 3D print 10.00 mm × 5.00 mm × 0.75 mm single-layer composite materials with evenly spaced parallel lines of aligned carbon microfibers (7.2 μm diameter, 100 μm length).^[104] They characterized the alignment of microfiber clusters (macroscale alignment) and individual microfibers (microscale alignment) (see **Figure 8f**) as a function of the fabrication process parameters (filler material weight percent [0.1–0.5], ultrasound transducer input voltage [30.5–51.6 V_{pp}], ultrasound transducer separation distance [18.0–36.0 wavelengths]) and found that macro- and microscale alignment can be unrelated to each other. Yunus et al. also used projection-based SLA with an ultrasound wave field within a hexagonal reservoir with three sets of parallel-oriented ultrasound transducers (2.33 MHz operating frequency) to align up to 9.0 wt% of CNFs (400 nm average diameter, 27.5 μm average length), magnetite nanoparticles (300 nm diameter), and copper nanoparticles (300 nm diameter) in 10 mm × 10 mm × 0.5 mm photopolymer resin specimens.^[26] They reported that electrical conductivity depends on both filler material weight percent and alignment. Lu et al. developed a combined projection-based SLA and ultrasound wave field method to fabricate composite material specimens (6 mm × 6 mm layers) based on two sets of parallel-oriented ultrasound transducers (43 kHz operating frequency) submerged in a resin vat with dispersed filler material (independent experiments with: spherical tungsten, aluminum, titanium, and copper particles with diameter between 70 nm and 75 μm).^[105] They cured single-layer specimens through selective UV light exposure, controlling the layer thickness using a moveable build plate. In a later study, Lu et al. used their fabrication method (see **Figure 8g**) to fabricate 7 mm × 7 mm × 5.4 mm thermally conductive composite material specimens comprising up to 30 photopolymer layers (45–90 μm layer thickness) with aluminum microparticles (30 μm diameter) and found that the heat dissipation of materials with aligned microparticles was ten times higher than with randomly oriented particles.^[20]

4. Operating Envelope, Limitations, and Applications of Combined Fabrication and Filler Material Alignment Methods

Table 1 shows a comparison between the different fabrication methods and each compatible filler alignment method, summarizing specimen length scale, print speed, resolution, and physical limitations. **Table 2** shows a comparison between the different filler material alignment methods, summarizing filler material size, filler material aspect ratio, filler material alignment

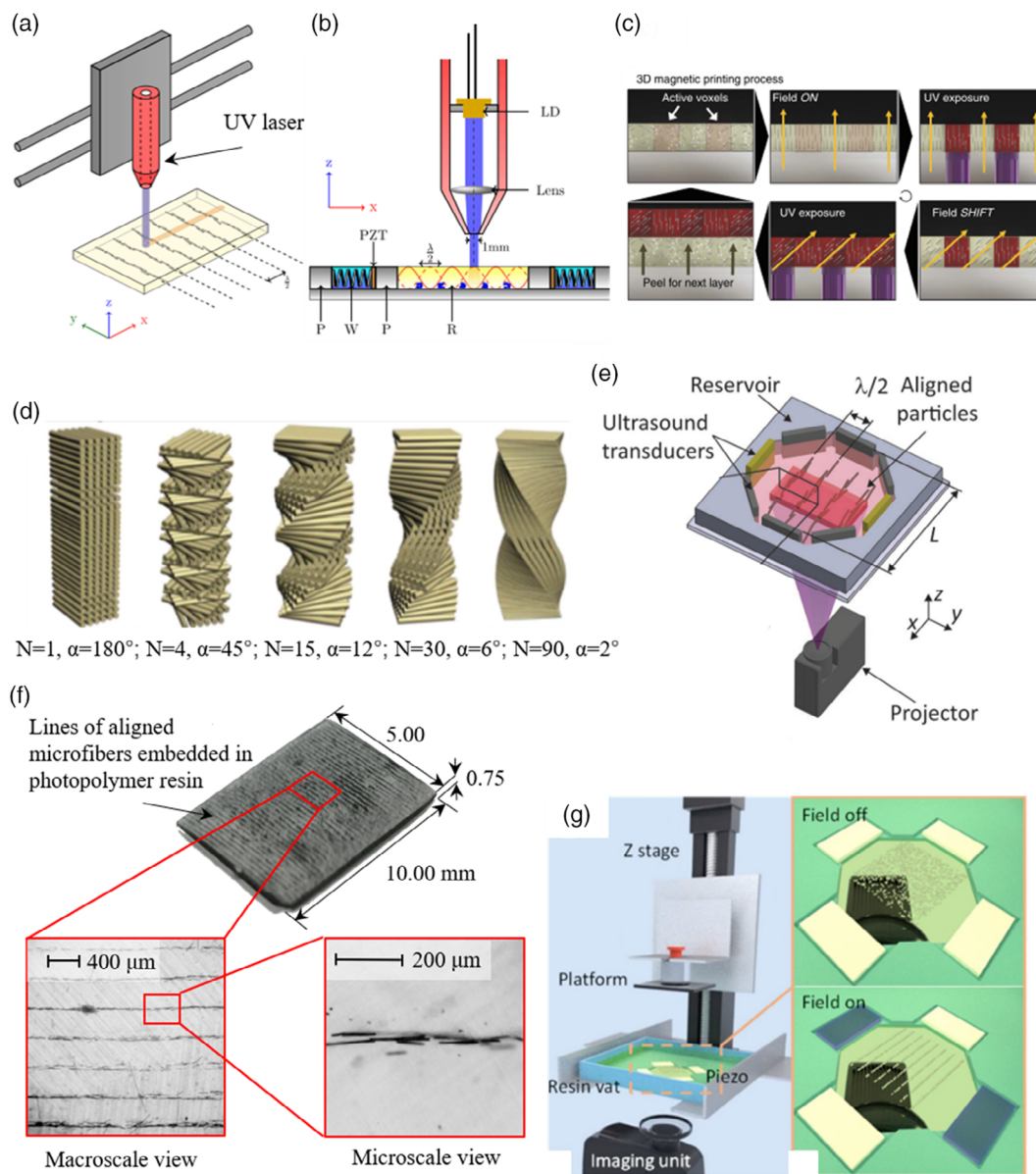


Figure 8. a) Schematic of a laser-based SLA printer that incorporates b) PZT (ultrasound) transducers to fabricate photopolymer composite material specimens with aligned filler material. Reproduced (adapted) with permission.^[101] Copyright 2016, IOP Publishing. c) Projection SLA and magnetic field fabrication process to systematically align and cure photopolymer composite material specimens with aligned filler material. Reproduced (adapted) with permission.^[21] Copyright 2015, Springer Nature. d) Schematic diagram of changing alignment angle increments in 90-layer composite material specimens. Reproduced (adapted) with permission.^[102] Copyright 2017, Wiley. e) Schematic of a projection-based SLA and an ultrasound wave field produced with an octagonal reservoir with four sets of parallel-oriented ultrasound transducers. Modified and reproduced (adapted) with permission.^[103] Copyright 2017, Wiley. f) 3D printed composite material specimen with lines of aligned microfibers with inset images showing aligned clusters of (macroscale) and individual (microscale) microfibers. g) Schematic of combined projection-based SLA and ultrasound wave field method to fabricate composite material specimens with aligned filler material. Reproduced (adapted) with permission.^[20] Copyright 2019, Elsevier.

time, field strength, filler material manipulation distance, material limitations, and physical limitations. **Figure 9** combines the information of Table 1 and 2 and visualizes the operating envelope of each combined fabrication and filler material alignment method, derived from the individual studies discussed in the previous section. We show the filler material weight percent w_f

versus the filler material aspect ratio for the different individual studies, where individual markers indicate single datapoints and lines cover a range of datapoints. The color and marker type indicate the filler material alignment method, whereas the shaded regions identify the bounds of the operating envelope for each fabrication method.

Table 1. Overview of fabrication methods documented in the literature, with citations to specific references, showing a setup schematic, compatible filler material alignment methods, size of printed specimens, minimum feature resolution, print speed and material limitations.

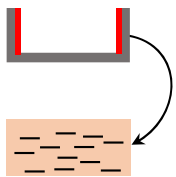
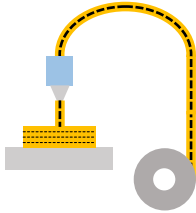
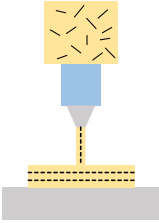
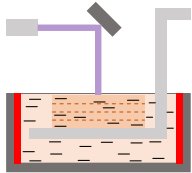
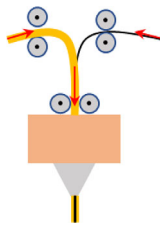
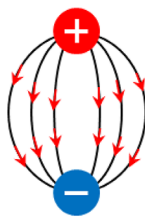
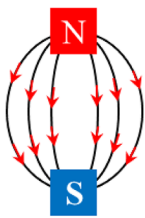
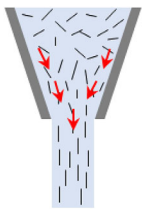
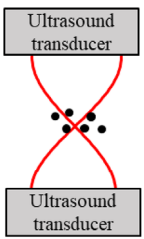
	Mold casting	FFF	DIW	SLA
Schematic				
Compatible filler material alignment methods	Electric field ^[8,24,34,38,53,56,57,108–110] Magnetic field ^[25,39,52,54,59,111–114] Ultrasound wave field ^[33,49,60]	Mechanical ^[64,65,67–69,79,80,83–87,107,115–135] Shear force field ^[63,66,70–74,136–142]	Shear force field ^[94–96] Magnetic field ^[97] Ultrasound wave field ^[46,91–93]	Electric field ^[102] Magnetic field ^[21] Ultrasound wave field ^[20,26,101,103–105]
Size of printed specimens	Hundreds of millimeters ^[57] (7.5 ^[33] –170 mm ^[57])	Hundreds of millimeters ^[68] (10 ^[80] –310 ^[68] mm)	Tens of millimeters ^[94] (8 ^[94] –57.5 ^[95] mm)	Tens of millimeters ^[21] (2 ^[101] –22 ^[21] mm)
Feature resolution	500 μm ^[60] –7 mm ^[25] specimen thickness	100 ^[79] –200 μm ^[140] layer thickness	200 ^[94] –500 μm ^[91] line width	90 μm ^[102] –1 mm ^[101] layer thickness
Print speed	N/A	1.7 ^[85] –280 mm s ⁻¹ ^[79]	1–20 mm s ⁻¹ ^[93]	Projector SLA: 2 ^[26] –18 ^[103] s curing/layer Laser SLA: 20 mm s ⁻¹ plus filler material alignment time ^[101]
Material limitations	Polymer matrix must be a thermoset	Polymer matrix must be a thermoplastic	Polymer matrix must be liquid resin and should be shear-thinning	Polymer matrix must be a photopolymer

Table 2. Overview of filler material alignment methods and their operating parameters documented in the literature, with citations to specific references.

	Mechanical force	Electric field	Magnetic field	Shear force field	Ultrasound wave field
Schematic					
Filler material size	Continuous with microscale-diameter fibers ^[69]	Nanoscale ^[34]	Nanoscale ^[112] to microscale ^[113]	Nanoscale ^[143] to microscale ^[96]	Nanoscale ^[49] to microscale ^[104]
Filler material aspect ratio	485 ^[69] –25714 ^[107]	4 ^[38] –9259 ^[56]	47 ^[21] –15577 ^[39]	22 ^[94] –533 ^[72]	1 (spherical) ^[93] –231 ^[49]
Filler material alignment time	Filler material aligns as it passes through an FFF extruder nozzle	Seconds ^[102] to tens of hours ^[57]	Seconds ^[21] to tens of hours ^[25]	N/A	Seconds ^[104]
Field strength	N/A	7.5 ^[53] –30 ^[102] V mm ⁻¹	40 ^[97] –8000 mT ^[41]	N/A	20 ^[46] V–100 V _{pp} ^[26] transducer operating voltage
Maximum filler material manipulation distance	Hundreds of millimeters ^[68]	Tens of millimeters ^[53]	Tens of millimeters ^[25]	N/A	Tens of millimeters ^[104]
Material limitations	Continuous filler material	Electrically conductive filler material	Ferromagnetic filler material	High-aspect-ratio filler material	Low-viscosity matrix
Physical limitations	Strands of filler material should be dispersed in matrix material	High field strength and long filler material alignment time	High field strength and long filler material alignment time	Filler material orientation controlled by matrix flow parameters	Matrix viscosity

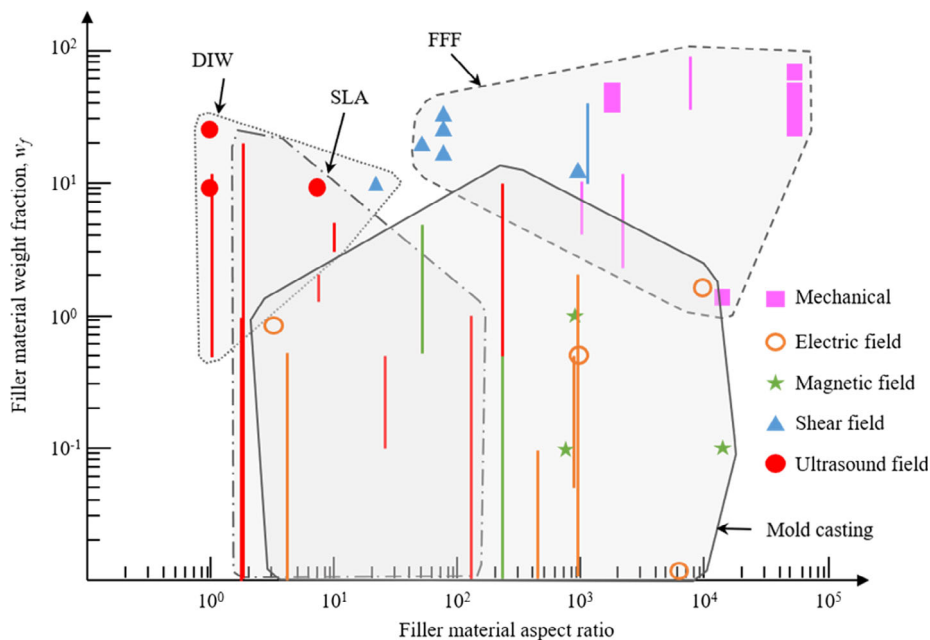


Figure 9. Filler material weight percent w_f versus filler material aspect ratio, indicating the operating envelope of each fabrication method (shaded regions) and filler material alignment method (color and marker style) discussed in this article.

4.1. Compatibility between Fabrication and Filler Material Alignment Methods

Mold casting combines with electric, magnetic, and ultrasound wave fields to align filler material. However, mold casting often does not provide intricate control of the material flow direction in the mold, which inhibits using shear force field filler material alignment. In contrast, FFF methods combine with mechanical force or shear force fields to align filler material during extrusion. However, no examples of FFF combined with electric, magnetic, or ultrasound wave field filler material alignment methods exist in the open literature. This is likely due to the high viscosity of liquid thermoplastic polymer resins and the fast print speed required in FFF methods because the nozzle traces the 3D contour of the specimen, thus limiting the time available to align the filler material. Polymer resin viscosity is an important consideration for all external field-directed filler material alignment methods because the driving force created by the external field must overcome the viscous drag force, thus inhibiting filler material alignment, but also keeping it from settling or precipitating.^[22] DIW fabrication methods show a slower print speed and use polymer resin materials with lower viscosity than FFF methods, thus enabling a magnetic or ultrasound wave field to align the filler material, in addition to a shear force field. However, the literature does not show any examples of DIW combined with an electric field. Theoretically, one could first print a specimen and then use an electric field to align the filler material or, alternatively, the DIW extruder nozzle could incorporate electrodes to align the filler material during the printing process. SLA fabrication methods use few moving parts and a large vat with a stationary photopolymer resin, which facilitates implementing an array of transducers to create an external

electric, magnetic, or ultrasound wave field. Because the photopolymer is stationary, SLA does not combine with a shear force field because it relies on polymer flow to align the filler material. Further, no publications exist that document SLA with mechanical alignment because it requires a moving printhead to introduce filler material in the liquid photopolymer, whereas SLA uses UV light exposure to define the specimen geometry.

4.2. Specimen Size

The fabrication method or filler material alignment method may constrain specimen size in different situations. Mechanical and shear force filler material alignment methods rely on material flow or extrusion to align the filler material during the fabrication process. Thus, the fabrication method only constrains the specimen geometry, not the filler material alignment method. In contrast, the specimen geometry when using an electric, magnetic, or ultrasound wave field filler material alignment method is typically limited by the alignment method rather than the fabrication method because the required field strength, and thus the transducer size and operating power, increases with increasing specimen geometry.

4.3. Resolution

The resolution of specimen geometry fabricated with mold casting depends on the accuracy and resolution of the mold itself as well as the viscosity of the liquid polymer resin, because the process requires the liquid resin taking the shape of the mold before it solidifies. Thus, if the resin viscosity is too high, it will not flow into intricate cavities or prevent forming high-resolution details, even if the mold itself has high-resolution features.

The resolution of specimen geometry fabricated with FFF methods depends on the type of filler material. For instance, when using mechanically aligned continuous filler material, the minimum radius of curvature of the brittle filler material dominates resolution. Chabaud et al. confirmed that the brittle behavior of continuous glass and carbon fibers limited specimen geometry resolution and reported that feature radii should be greater than 0.62 mm to avoid damage to the continuous carbon fibers.^[83] In contrast, when using a discontinuous filler material aligned using shear force fields during FFF, the length scale of individual filler material particles is typically much smaller than the radius of curvature of each filament strand, rendering brittle behavior less relevant in terms of specimen geometry. Therefore, the fabrication process parameters, including layer thickness, extruder nozzle diameter, and extruder nozzle geometry, limit the resolution of the specimen geometry.

DIW fabrication methods use an extruder nozzle to deposit lines of liquid resin with aligned filler material. The extruder nozzle diameter, polymer matrix viscosity, and polymer matrix shape-retaining characteristics, which derive from the chemical composition of the ink,^[93] limit the specimen geometry resolution. The requirements of external field filler material alignment methods could further limit the diameter of the extruder nozzle. For instance, DIW methods combined with an ultrasound wave field must accommodate ultrasound transducers to establish a standing ultrasound wave, which depends on factors including the ultrasound transducer operating frequency, and resin and filler material properties.

SLA fabrication methods rely on selectively curing a photopolymer using UV light, and the spatial and temporal application of UV photons determines the specimen geometry resolution, in addition to the light-scattering characteristics of the photopolymer resin.^[100] Yang et al. used projection SLA and reported a minimum feature resolution of 90 μm ,^[102] which is the lowest of all fabrication methods in this review.

4.4. Print Speed

Print speed varies from 1^[93] to 280 mm s^{-1} ^[79] for extrusion or laser SLA fabrication methods and from 2^[26] to 18^[103] s per layer for projector SLA, depending on the fabrication setup and filler material alignment method.

The fabrication method, not the filler material alignment method, limits the FFF print speed because the filler material aligns quasi-instantaneously as a result of mechanical force (continuous filler material) or shear forces (discontinuous filler material) during extrusion. Thus, controlling the filament feed rate and the heat transfer rate between the heated extruder nozzle and the thermoplastic resin allows managing throughput and enables print speeds as high as 280 mm s^{-1} ^[79] for a continuous filler material and 50 mm s^{-1} ^[74] for a discontinuous filler material.

DIW fabrication methods often display a complex setup that incorporates multiple filler and/or matrix materials. Further, they may involve separate steps to extrude the mixture of matrix and filler materials, align the filler material, and cure the matrix material. As a result, DIW print speeds range from 1 to 20 mm s^{-1} ,^[93] which is substantially slower than FFF and laser SLA fabrication methods.

SLA print speeds are as fast as 20 mm s^{-1} for laser SLA^[101] and 2 s layer⁻¹ for projector SLA.^[26] The filler material alignment method typically limits the projector SLA print speed because an entire layer of photopolymer cures at once in seconds. Further, SLA combines with electric and magnetic fields which require long filler material alignment times, up to tens of hours for [25] and [57], respectively, compared to only seconds for ultrasound wave fields,^[104] which limits the print speed.

4.5. Compatible Filler Materials

Filler materials in polymer matrix composite materials vary greatly in size, aspect ratio, weight percent, and composition, with substantial overlap in compatibility between filler material alignment and fabrication methods (see Figure 9). Mechanical alignment methods require an extruder nozzle to instantaneously align continuous filler material. Shear force fields require high aspect ratio filler material because the force from the shear force field, which decreases with increasing filler material alignment in the shear direction, exerts pressure on the filler material orthogonal to the shear direction.^[42] Increasing the filler material weight percent increases viscosity and drag force and requires increasing the magnitude of the external field. Thus, the filler material weight percent is typically low when using an electric, magnetic, or ultrasound wave field.^[49]

Mold casting combines with nano- or microscale filler material and displays a larger operating envelope in terms of filler material weight percent and aspect ratio (see Figure 9) than FFF, DIW, and SLA because it combines with three types of external field filler material alignment methods.

FFF combines with continuous carbon, glass, or Kevlar fibers (microscale fiber diameter) or chopped macro- or microscale carbon fibers. FFF methods allow higher filler material weight percent than mold casting, DIW, and SLA (see Figure 9) because an extruder nozzle can directly place in highly viscous resin with less concern for consistent filler material dispersion or settling. Further, the filler material aspect ratio can be much larger than for mold casting, DIW, and SLA because the effective filler material length equates to the specimen length when using mechanically aligned continuous fibers.

DIW combines with nano- and microscale filler material, and often shows a higher filler material weight percent than mold casting and SLA methods (see Figure 9) because shear-thinning inks increase viscosity after deposition, thus reducing filler material settling.

SLA fabrication methods combine with nano- and microscale filler materials, and use filler material weight percent and aspect ratio that overlap with DIW and mold casting (see Figure 9) because many filler material alignment methods that combine with SLA also combine with either mold casting or DIW. However, high filler material weight percent is difficult to achieve with SLA because it inhibits UV light penetration into the resin, thus inhibiting resin curing during fabrication.

4.6. Filler Material Alignment Distance and Degree of Alignment

The filler material manipulation distance and degree of alignment vary significantly for different filler material alignment

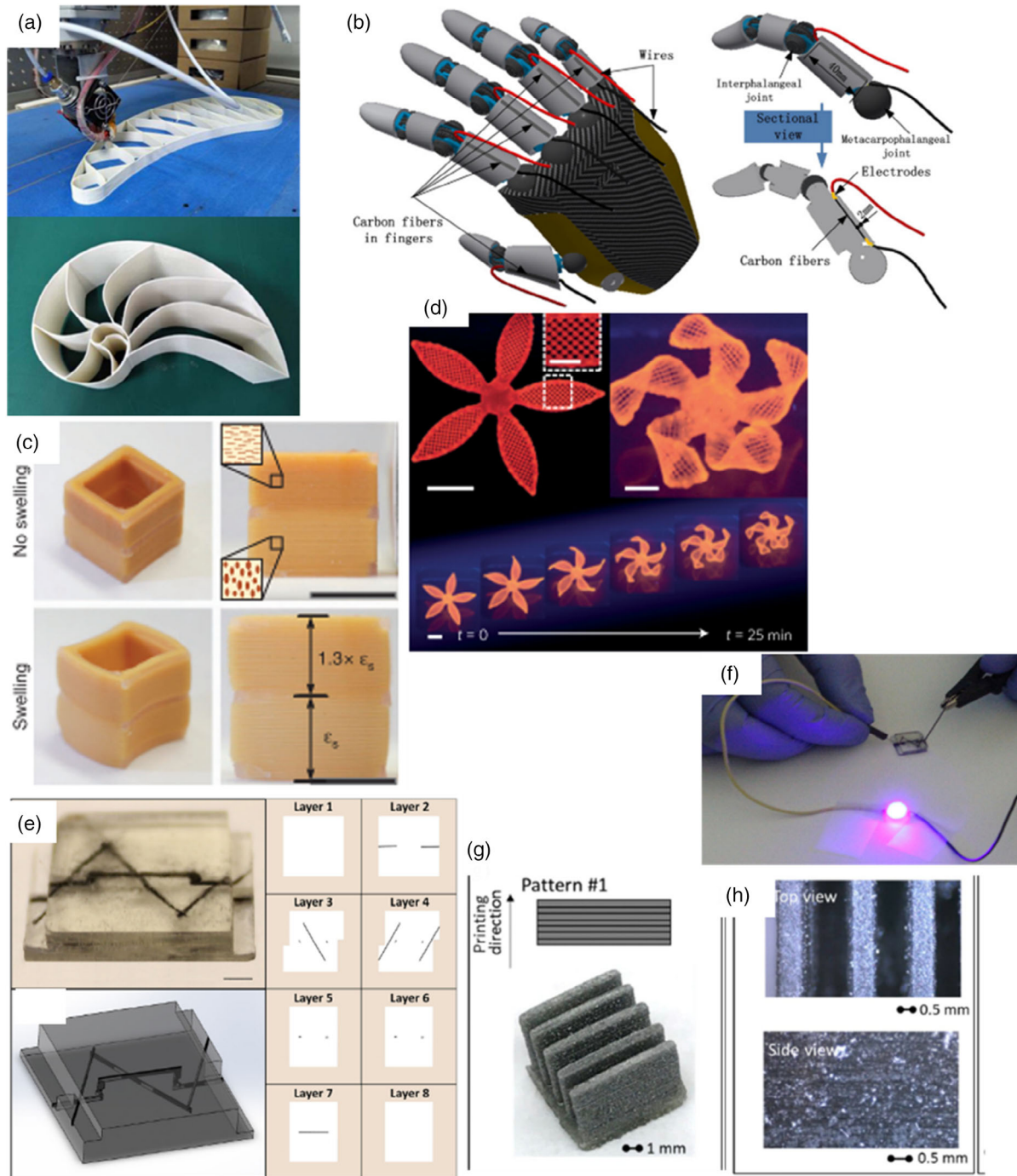


Figure 10. a) Heterogeneous sandwich composite structure fabricated using FFF with a continuous fiber bundle mechanically aligned inside the thermoplastic body, optimized for maximum compressive strength. Modified and reproduced (adapted) with permission.^[85], Copyright 2018, Elsevier. b) Piezoresistive robot hand with carbon fiber mechanically aligned in PLA using FFF. Reproduced (adapted) with permission.^[107] Copyright 2017, Elsevier. c) Shape-changing cuboid fabricated using DIW with multiple inks and platelets vertically and horizontally aligned using a magnetic field.^[97] d) DIW printed flower with leaves that curl in response to anisotropic swelling resulting from cellulose fibers aligned using a shear force field.^[95] e) Embedded wire formed by aligning nanoparticles, using an ultrasound wave field, in an eight-layer SLA-printed composite material and f) demonstration of electrical conductivity of (e) through LED illumination. Modified and reproduced with permission.^[26] Copyright 2017, IOP Publishing. g) Isometric, h) top, and side view of a 15-layer heat sink, printed using SLA, with microscale aluminum powder aligned using an ultrasound wave field. Modified and reproduced (adapted) with permission.^[20] Copyright 2019, Elsevier.

methods. A computer-controlled extruder nozzle determines the location and alignment of continuous filler material, which enables quasi-instantaneous filler material manipulation over hundreds of millimeters in complex patterns.^[68] Mechanical control of continuous strands of filler material yields the highest degree of alignment of all filler material alignment methods in this review.

In contrast, electric, magnetic, and ultrasound wave fields only allow manipulating and aligning filler material over a distance of the order of tens of millimeters because the external field strength poses a physical limitation. Consequently, the external field strength also limits the degree of alignment because it may not overcome viscous drag or filler material entanglement. For example, Niendorf and Raeymaekers found the degree of alignment of carbon microfibers in an ultrasound wave field to decrease with increasing filler weight percent because microfibers entangle with each other, physically preventing them from aligning in the desired orientation.^[104]

Magnetic fields rely on current flow, whereas electric fields rely on voltage potential. Therefore, electric fields are more viable than magnetic fields because of the physical solenoid wire size, material limitations, and heat dissipation. Publications rarely report ultrasound wave field pressure, but ultrasound transducer operating voltage varies from 20^[46] to 100 V_{pp}.^[26] Regression analysis of the specifications found in the publications that use ultrasound wave field alignment shows that filler material length increases with increasing ultrasound transducer operating voltage, suggesting that aligning filler material requires increasing power with increasing size. Regression analysis did not reveal trends between filler material characteristics and field strength for electric or magnetic fields.

Shear force fields rely on material flow (liquid specimen) or strain (solid specimen) to orient discontinuous filler material particles, typically in the shear direction. However, shear force field alignment methods cannot spatially manipulate filler material, resulting in limited control compared to alignment methods that use a mechanical force or external field. Further, shear force field alignment methods are highly dependent on the shear rate, where the degree of filler material alignment increases with increasing shear rate.^[106]

4.7. Applications of Polymer Matrix Composite Materials with Aligned Filler Material

Figure 10 shows a selection of polymer matrix composite materials with spatially organized and/or aligned filler material specifically fabricated for use in a selection of engineering applications. Figure 10a shows a heterogeneous lightweight sandwich composite structure fabricated using a continuous fiber bundle inside a 60 mm × 60 mm × 15 mm thermoplastic body using FFF, optimized for maximum compressive strength, for use in e.g., the aerospace industry.^[85] The FFF fabrication process, combined with mechanical filler material alignment, enabled printing specimens of the order of tens of millimeters with varying printing process parameters, including cell size, specimen density, and layer thickness. Figure 10b shows a piezoresistive PLA robot hand with precisely embedded continuous carbon fibers, fabricated using FFF, essentially creating

materials with embedded sensing.^[107] The FFF process allowed printing of mechanically aligned carbon fiber bundles preimpregnated with epoxy resin, which increased strength and stiffness by 70% and 18.7%, respectively, compared to virgin PLA specimens. Figure 10c shows a cuboid that exhibits shape change in response to anisotropic swelling, which results from DIW with soft and stiff inks containing anisotropic patterns of alumina platelets aligned horizontally in the top section and vertically in the bottom section using a magnetic field.^[97] Similarly, Figure 10d shows the leaves of a 3D printed flower curl as a function of time in response to anisotropic swelling, which results from alternating layers of cellulose fibers aligned in different directions using a shear force field.^[95] These shape-shifting, multimaterial composite materials are relevant to creating designer shape-changing materials for soft robotics or biomedical devices. Figure 10e shows an embedded zig-zag nanoparticle wire in an eight-layer composite material fabricated using projection-based SLA, which enabled electrical conductivity between layers in the thickness direction, and an ultrasound wave field, which enabled electrical conductivity across each layer.^[26] Figure 10f shows the electrical conductivity of Figure 10e through light-emitting diode (LED) illumination and is relevant for embedding electrical wiring in structural materials, sensors, and flexible electronics. Figure 10g,h shows a 3D printed heat sink fabricated with SLA using 15 layers of microscale aluminum powder aligned in a photopolymer using an ultrasound wave field.^[20] Ultrasound wave alignment facilitates adjusting the patterns of embedded filler material, enabling tunable heat dissipation efficiency, and making it appropriate for addressing thermal challenges in 3D printed electronics and biomedical applications.

5. Conclusion

Additive manufacturing methods, such as FFF or FDM, DIW, and SLA, offer significant advantages over conventional mold casting fabrication methods because they enable fabricating complex polymer matrix composite material specimen geometries without the use of a mold. Combining additive manufacturing methods with a filler material alignment method allows spatially organizing and orienting continuous or discontinuous filler material, using mechanical force or an external, electric, magnetic, shear force, or ultrasound wave field. This facilitates fabricating polymer matrix composite materials with designer properties that depend on the properties of, and interaction between, the matrix and filler material as well as the spatial distribution and orientation of the filler material in the matrix. These fabrication and filler material alignment methods require sensitive tuning, which remains a challenge to scaling toward a mass manufacturing process. However, their ability to fabricate engineered polymer composite materials with designer material properties demonstrates significant advantages and promise compared to conventional fabrication methods.

Numerous publications document applications of such engineered polymer matrix composite materials, including flexible electronics, shape-changing structures, and structural components, that showcase how specific materials are fabricated as well

as their resulting properties. Choosing a fabrication and filler material alignment method out of the many possible combinations depends on the desired specimen geometry and size, resolution, print speed, filler material alignment time, polymer matrix and filler material requirements, and filler material manipulation requirements for any specific material application.

Acknowledgements

This research was supported by the National Science Foundation under award nos. 1636208 and 2017588.

Conflict of Interest

The authors declare no conflict of interest.

Keywords

additive manufacturing, aligned filler materials, directed self-assembly, microcomposite materials, nanocomposite materials

Received: August 25, 2020

Revised: November 23, 2020

Published online:

- [1] S.-J. Park, M.-K. Seo, *Interface Science and Technology*, Vol. 18, Elsevier, Amsterdam **2011**, p. 501–629.
- [2] U. Kalsoom, P. N. Nesterenko, B. Paull, *RSC Adv.* **2016**, 6, 60355.
- [3] P. C. Ma, N. A. Siddiqui, G. Marom, J. K. Kim, *Compos. A Appl. Sci. Manuf.* **2010**, 41, 1345.
- [4] X. L. Xie, Y. W. Mai, X. P. Zhou, *Mater. Sci. Eng. R Rep.* **2005**, 49, 89.
- [5] K. Joseph, S. K. Malhotra, K. Goda, M. S. Sreekala, *Polym. Compos.* **2012**, 1, 1.
- [6] A. K.-T. Lau, D. Hui, *Compos. B Eng.* **2002**, 33, 263.
- [7] S. Wickramasinghe, T. Do, P. Tran, *Polymers* **2020**, 12, 1529.
- [8] S. U. Khan, J. R. Pothnis, J. K. Kim, *Compos. A Appl. Sci. Manuf.* **2013**, 49, 26.
- [9] J. E. Fischer, W. Zhou, J. Vavro, M. C. Llaguno, C. Guthy, R. Haggemueller, M. J. Casavant, D. E. Walters, R. E. Smalley, *J. Appl. Phys.* **2003**, 93, 2157.
- [10] L. Tong, A. P. Mouritz, M. Bannister, *3D Fibre Reinforced Polymer Composites*, Elsevier Science & Technology, Oxford **2002**.
- [11] J. Delmonte, *Metal Composites*, Springer, Boston **1990**.
- [12] E. G. Kim, J. K. Park, S. H. Jo, *J. Mater. Process. Technol.* **2001**, 111, 225.
- [13] I. Gibson, D. Rosen, B. Stucker, *Additive Manufacturing Technologies: 3D Printing, Rapid Prototyping, and Direct Digital Manufacturing*, Springer, Berlin **2015**.
- [14] W. Gao, Y. Zhang, D. Ramanujan, K. Ramani, Y. Chen, C. B. Williams, C. C. L. Wang, Y. C. Shin, S. Zhang, P. D. Zavattieri, *CAD Comput. Aided Des.* **2015**, 69, 65.
- [15] P. S. Goh, A. F. Ismail, B. C. Ng, *Composites, Part A* **2014**, 56, 103.
- [16] B. Brenken, E. Barocio, A. Favaloro, V. Kunc, R. B. Pipes, *Addit. Manuf.* **2018**, 21, 1.
- [17] G. D. Goh, Y. L. Yap, S. Agarwala, W. Y. Yeong, *Adv. Mater. Technol.* **2019**, 4, 1800271.
- [18] T. Sugama, K. Gawlik, *Polym. Polym. Compos.* **2003**, 11, 161.
- [19] A. Thankappan, S. Thomas, V. P. N. Nampoori, *Opt. Laser Technol.* **2014**, 58, 63.
- [20] L. Lu, Z. Zhang, J. Xu, Y. Pan, *Composites, Part B* **2019**, 174, 106991.
- [21] J. J. Martin, B. E. Fiore, R. M. Erb, *Nat. Commun.* **2015**, 6, 8641.
- [22] M. Roy, P. Tran, T. Dickens, A. Schrand, *J. Compos. Sci.* **2019**, 4, 1.
- [23] N. P. Singh, V. K. Gupta, A. P. Singh, *Polymer* **2019**, 180, 121724.
- [24] R. B. Ladani, S. Wu, A. J. Kinloch, K. Ghorbani, J. Zhang, A. P. Mouritz, C. H. Wang, *Mater. Des.* **2016**, 94, 554.
- [25] S. Wu, J. Zhang, R. B. Ladani, K. Ghorbani, A. P. Mouritz, A. J. Kinloch, C. H. Wang, *Polymer* **2016**, 97, 273.
- [26] D. E. Yunus, S. Sohrabi, R. He, W. Shi, Y. Liu, *J. Micromech. Microeng.* **2017**, 27, 045016.
- [27] S. M. F. Kabir, K. Mathur, A. F. M. Seyam, *Compos. Struct.* **2020**, 232, 111476.
- [28] Z. M. Huang, Y. Z. Zhang, M. Kotaki, S. Ramakrishna, *Compos. Sci. Technol.* **2003**, 63, 2223.
- [29] P. Pötschke, H. Brüning, A. Janke, D. Fischer, D. Jehnichen, *Polymer* **2005**, 46, 10355.
- [30] S. Zhang, K. K. K. Koziol, I. A. Kinloch, A. H. Windle, *Small* **2008**, 4, 1217.
- [31] Y. L. Li, I. A. Kinloch, A. H. Windle, *Science* **2004**, 304, 276.
- [32] M. Moniruzzaman, K. I. Winey, *Macromolecules* **2006**, 39, 5194.
- [33] J. Greenhall, L. J. Homel, B. Raeymaekers, *J. Compos. Mater.* **2018**, 53, 1329.
- [34] P. Gupta, M. Rajput, N. Singla, V. Kumar, D. Lahiri, *Polymer* **2016**, 89, 119.
- [35] J. Hone, M. C. Llaguno, N. M. Nemes, A. T. Johnson, J. E. Fischer, D. A. Walters, M. J. Casavant, J. Schmidt, R. E. Smalley, *Appl. Phys. Lett.* **2000**, 77, 666.
- [36] D. S. Melchert, R. R. Collino, T. R. Ray, N. Dolinski, L. Friedrich, M. R. Begley, D. S. Gianola, *Adv. Mater. Technol.* **2019**, 4, 1900586.
- [37] Q. Wang, J. Dai, W. Li, Z. Wei, J. Jiang, *Compos. Sci. Technol.* **2008**, 68, 1644.
- [38] A. I. Oliva-Avilés, F. Avilés, V. Sosa, A. I. Oliva, F. Gamboa, *Nanotechnology* **2012**, 23, 465710.
- [39] A. Sharma, B. Tripathi, Y. K. Vijay, *J. Memb. Sci.* **2010**, 361, 89.
- [40] P. V. Kamat, K. G. Thomas, S. Barazzouk, G. Girishkumar, K. Vinodgopal, D. Meisel, *J. Am. Chem. Soc.* **2004**, 126, 10757.
- [41] Y. Tanimoto, M. Fujiwara, Y. Shimomura, I. Mukouda, E. Oki, M. Hamada, *J. Phys. Chem. A* **2002**, 105, 4383.
- [42] D. Z. Gunes, R. Scirocco, J. Mewis, J. Vermant, *J. Nonnewton. Fluid Mech.* **2008**, 155, 39.
- [43] P. M. Ajayan, O. Stephan, C. Colliex, D. Trauth, *Science* **1994**, 265, 1212.
- [44] M. Prisbrey, J. Greenhall, F. Guevara Vasquez, B. Raeymaekers, *J. Appl. Phys.* **2017**, 121, 014302.
- [45] M. Prisbrey, B. Raeymaekers, *Phys. Rev. Appl.* **2019**, 12, 014014.
- [46] R. R. Collino, T. R. Ray, R. C. Fleming, C. H. Sasaki, H. Haj-Hariri, M. R. Begley, *Extrem. Mech. Lett.* **2015**, 5, 37.
- [47] L. E. Kinsler, A. R. Frey, A. B. Coppens, J. V. Sanders, *Fundamentals of Acoustics*, John Wiley, New York **2000**.
- [48] H. H. Gommans, J. W. Alldredge, H. Tashiro, J. Park, J. Magnuson, A. G. Rinzler, *J. Appl. Phys.* **2000**, 88, 2509.
- [49] M. D. Haslam, B. Raeymaekers, *Composites, Part B* **2014**, 60, 91.
- [50] J. J. Hermans, P. H. Hermans, D. Vermaas, A. Weidinger, *Recl. Des Trav. Chim. Des Pays-Bas* **1946**, 65, 427.
- [51] C. E. Ayres, B. S. Jha, H. Meredith, J. R. Bowman, G. L. Bowlin, S. C. Henderson, D. G. Simpson, *J. Biomater. Sci. Polym. Edn.* **2008**, 19, 603.
- [52] M. Abdalla, D. Dean, M. Theodore, J. Fielding, E. Nyairo, G. Price, *Polymer* **2010**, 51, 1614.
- [53] J. R. Pothnis, S. Gururaja, D. Kalyanasundaram, *Mech. Adv. Mater. Struct.* **2019**, 26, 35.
- [54] R. M. Erb, J. Segmehl, M. Charilaou, J. F. Löffler, A. R. Studart, *Soft Matter* **2012**, 8, 7604.
- [55] M. L. Sham, J. K. Kim, *Carbon* **2006**, 44, 768.

- [56] R. B. Ladani, S. Wu, A. J. Kinloch, K. Ghorbani, J. Zhang, A. P. Mouritz, C. H. Wang, *Compos. Sci. Technol.* **2015**, *117*, 146.
- [57] S. Wu, R. B. Ladani, A. R. Ravindran, J. Zhang, A. P. Mouritz, A. J. Kinloch, C. H. Wang, *Compos. Sci. Technol.* **2017**, *152*, 46.
- [58] H. Morgan, N. G. Green, *AC Electrokinetics: Colloids and Nanoparticles*, Research Studies Press, Philadelphia, PA **2003**.
- [59] R. M. Erb, J. S. Sander, R. Grisch, A. R. Studart, *Nat. Commun.* **2013**, *4*, 1.
- [60] M. S. Scholz, B. W. Drinkwater, R. S. Trask, *Ultrasonics* **2014**, *54*, 1015.
- [61] C. K. Chau, K. F. Leong, *3D Printing and Additive Manufacturing: Principles and Applications*, World Scientific, Singapore **2015**.
- [62] L. G. Blok, M. L. Longana, H. Yu, B. K. S. Woods, *Addit. Manuf.* **2018**, *22*, 176.
- [63] W. Zhang, C. Cotton, J. Sun, D. Heider, B. Gu, B. Sun, T. W. Chou, *Composites, Part B* **2018**, *137*, 51.
- [64] N. van de Werken, J. Hurley, P. Khanbolouki, A. N. Sarvestani, A. Y. Tamijani, M. Tehrani, *Composites, B* **2019**, *160*, 684.
- [65] R. Matsuzaki, M. Ueda, M. Namiki, T. K. Jeong, H. Asahara, K. Horiguchi, T. Nakamura, A. Todoroki, Y. Hirano, *Sci. Rep.* **2016**, *6*, 23058.
- [66] M. Spoerk, C. Savandaiah, F. Arbeiter, G. Traxler, L. Cardon, C. Holzer, J. Sapkota, *Composites, Part B* **2018**, *113*, 95.
- [67] X. Tian, T. Liu, Q. Wang, A. Dilmurat, D. Li, G. Ziegmann, *J. Clean. Prod.* **2017**, *142*, 1609.
- [68] J. Justo, L. Távora, L. García-Guzmán, F. París, *Compos. Struct.* **2018**, *185*, 537.
- [69] G. W. Melenka, B. K. O. Cheung, J. S. Schofield, M. R. Dawson, J. P. Carey, *Compos. Struct.* **2016**, *153*, 866.
- [70] L. J. Love, V. Kunc, O. Rios, C. E. Duty, A. M. Elliott, B. K. Post, R. J. Smith, C. A. Blue, *J. Mater. Res.* **2014**, *29*, 1893.
- [71] M. L. Shofner, K. Lozano, F. J. Rodríguez-Macías, E. V. Barrera, *J. Appl. Polym. Sci.* **2003**, *89*, 3081.
- [72] H. L. Tekinalp, V. Kunc, G. M. Velez-Garcia, C. E. Duty, L. J. Love, A. K. Naskar, C. A. Blue, S. Ozcan, *Compos. Sci. Technol.* **2014**, *105*, 144.
- [73] T. Mulholland, S. Goris, J. Boxleitner, T. A. Osswald, N. Rudolph, *Addit. Manuf. Compos. Complex Mater.* **2018**, *70*, 298.
- [74] R. T. L. Ferreira, I. C. Amatte, T. A. Dutra, D. Bürger, *Composites, B* **2017**, *124*, 88.
- [75] Markforged Inc., Material Data Sheet: Composites, https://static.markforged.com/markforged_composites_datasheet.pdf (accessed: May 2020).
- [76] S. G. Advani, C. L. I. Tucker, *J. Rheol.* **1987**, *31*, 751.
- [77] N. Mohan, P. Senthil, S. Vinodh, N. Jayanth, *Virtual Phys. Prototyp.* **2017**, *12*, 47.
- [78] G. T. Mark, A. S. Gozdz, US20140291886A1 **2014**.
- [79] [G. T. Mark, A. S. Gozdz, US9149988B2 **2015**.
- [80] M. A. Caminero, J. M. Chacón, I. García-Moreno, G. P. Rodríguez, *Compos.* **2018**, *148*, 93.
- [81] L. Pyl, K. A. Kalteremidou, D. Van Hemelrijck, *Compos. Sci. Technol.* **2019**, *171*, 135.
- [82] J. Naranjo-Lozada, H. Ahuett-Garza, P. Orta-Castañón, W. M. H. Verbeeten, D. Sáiz-González, *Addit. Manuf.* **2019**, *26*, 227.
- [83] G. Chabaud, M. Castro, C. Denoual, A. Le Duigou, *Addit. Manuf.* **2019**, *26*, 94.
- [84] X. Tian, T. Liu, C. Yang, Q. Wang, D. Li, *Composites, Part A* **2016**, *88*, 198.
- [85] Z. Hou, X. Tian, J. Zhang, D. Li, *Compos. Struct.* **2018**, *184*, 1005.
- [86] N. Li, Y. Li, S. Liu, *J. Mater. Process. Technol.* **2016**, *238*, 218.
- [87] M. Heidari-Rarani, M. Rafiee-Afarani, A. M. Zahedi, *Composites, Part B* **2019**, *175*, 107147.
- [88] R. D. Farahani, M. Dubé, D. Therriault, *Adv. Mater.* **2016**, *28*, 5794.
- [89] J. E. Smay, J. Cesarano, J. A. Lewis, *Langmuir* **2002**, *18*, 5429.
- [90] C. Zhu, J. E. Smay, *J. Mater. Process. Technol.* **2012**, *212*, 727.
- [91] R. R. Collino, T. R. Ray, R. C. Fleming, J. D. Cornell, B. G. Compton, M. R. Begley, *Extrem. Mech. Lett.* **2016**, *8*, 96.
- [92] P. Wadsworth, I. Nelson, D. L. Porter, B. Raeymaekers, S. E. Naleway, *Mater. Des.* **2020**, *185*, 108243.
- [93] L. Friedrich, R. Collino, T. Ray, M. Begley, *Sens. Actuators Phys.* **2017**, *268*, 213.
- [94] B. G. Compton, J. A. Lewis, *Adv. Mater.* **2014**, *26*, 5930.
- [95] S. A. Gladman, E. A. Matsumoto, R. G. Nuzzo, L. Mahadevan, J. A. Lewis, *Nat. Mater.* **2016**, *15*, 413.
- [96] J. P. Lewicki, J. N. Rodriguez, C. Zhu, M. A. Worsley, A. S. Wu, Y. Kanarska, J. D. Horn, E. B. Duoss, J. M. Ortega, W. Elmer, R. Hensleigh, R. A. Fellini, M. J. King, *Sci. Rep.* **2017**, *7*, 43401.
- [97] D. Kokkinis, M. Schaffner, A. R. Studart, *Nat. Commun.* **2015**, *6*, 8643
- [98] M. M. Emami, F. Barazandeh, F. Yaghmaie, *J. Mater. Process. Technol.* **2015**, *219*, 17.
- [99] J. Valentinčič, M. Peroša, M. Jerman, I. Sabotin, A. Lebar, *Stroj. Vestnik/J. Mech. Eng.* **2017**, *63*, 559.
- [100] J. Z. Manapat, Q. Chen, P. Ye, R. C. Advincula, *Macromol. Mater. Eng.* **2017**, *302*, 1600553.
- [101] T. M. Llewellyn-Jones, B. W. Drinkwater, R. S. Trask, *Smart Mater. Struct.* **2016**, *25*, 02LT01.
- [102] Y. Yang, Z. Chen, X. Song, Z. Zhang, J. Zhang, K. K. Shung, Q. Zhou, Y. Chen, *Adv. Mater.* **2017**, *29*, 1605750.
- [103] J. Greenhall, B. Raeymaekers, *Adv. Mater. Technol.* **2017**, *2*, 1700122.
- [104] K. Niendorf, B. Raeymaekers, *Composites, Part A* **2020**, *129*, 105713.
- [105] L. Lu, X. Tang, S. Hu, Y. Pan, *3D Print. Addit. Manuf.* **2018**, *5*, 151.
- [106] A. B. Sulong, J. Park, *J. Compos. Mater.* **2011**, *45*, 931.
- [107] X. Yao, C. Luan, D. Zhang, L. Lan, J. Fu, *Mater. Des.* **2017**, *114*, 424.
- [108] W. A. Chapkin, D. Q. McNerny, M. F. Aldridge, Y. He, W. Wang, J. Kieffer, A. I. Taub, *Polym. Test.* **2016**, *56*, 29.
- [109] W. A. Chapkin, J. K. Wenderott, P. F. Green, A. I. Taub, *Carbon* **2018**, *131*, 275.
- [110] E. S. Choi, J. S. Brooks, D. L. Eaton, M. S. Al-Haik, M. Y. Hussaini, H. Garmestani, D. Li, K. Dahmen, *J. Appl. Phys.* **2003**, *94*, 6034.
- [111] R. M. Erb, K. H. Cherenack, R. E. Stahel, R. Libanori, T. Kinkeldei, N. Münzenrieder, G. Tröster, A. R. Studart, *ACS Appl. Mater. Interfaces* **2012**, *4*, 2860.
- [112] C. Ma, H. Y. Liu, X. Du, L. Mach, F. Xu, Y. W. Mai, *Compos. Sci. Technol.* **2015**, *114*, 126.
- [113] R. Libanori, R. M. Erb, A. R. Studart, *ACS Appl. Mater. Interfaces* **2013**, *5*, 10794.
- [114] R. M. Erb, R. Libanori, N. Rothfuchs, A. R. Studart, *Science* **2012**, *335*, 199.
- [115] F. Van Van Der Klift, Y. Koga, A. Todoroki, M. Ueda, Y. Hirano, R. Matsuzaki, *Open J. Compos. Mater.* **2016**, *06*, 18.
- [116] Y. Peng, Y. Wu, K. Wang, G. Gao, S. Ahzi, *Compos. Struct.* **2019**, *207*, 232.
- [117] Y. Peng, Y. Wu, S. Li, K. Wang, S. Yao, Z. Liu, H. Garmestani, *Compos. Sci. Technol.* **2020**, *199*, 108337.
- [118] G. Dong, Y. Tang, D. Li, Y. F. Zhao, *Procedia Manuf.* **2018**, *26*, 774.
- [119] M. Mohammadzadeh, A. Imeri, I. Fidan, M. Elkelany, *Composites, Part B* **2019**, *175*, 107112.
- [120] T. Liu, X. Tian, M. Zhang, D. Abliz, D. Li, G. Ziegmann, *Composites, Part A* **2018**, *114*, 368.
- [121] F. Akasheh, H. Aglan, *J. Elastomers Plast.* **2019**, *51*, 698.
- [122] H. Al Abadi, H. T. Thai, V. Paton-Cole, V. I. Patel, *Compos. Struct.* **2018**, *193*, 8.
- [123] C. Oztan, R. Karkkainen, M. Fittipaldi, G. Nygren, L. Roberson, M. Lane, E. Celik, *J. Compos. Mater.* **2019**, *53*, 271.
- [124] A. Le Duigou, A. Barbé, E. Guillou, M. Castro, *Mater. Des.* **2019**, *180*, 107884.

- [125] B. Akhouni, A. H. Behraves, A. Bagheri Saed, *J. Reinf. Plast. Compos.* **2019**, *38*, 99.
- [126] K. Sugiyama, R. Matsuzaki, A. V. Malakhov, A. N. Polilov, M. Ueda, A. Todoroki, Y. Hirano, *Compos. Sci. Technol.* **2020**, *186*, 107905.
- [127] Q. He, H. Wang, K. Fu, L. Ye, *Compos. Sci. Technol.* **2020**, *191*, 108077.
- [128] K. Agarwal, S. K. Kuchipudi, B. Girard, M. Houser, *J. Compos. Mater.* **2018**, *52*, 3173.
- [129] G. D. Goh, V. Dikshit, A. P. Nagalingam, G. L. Goh, S. Agarwala, S. L. Sing, J. Wei, W. Y. Yeong, *Mater. Des.* **2018**, *137*, 79.
- [130] C. Luan, X. Yao, C. Zhang, B. Wang, J. Fu, *Compos. Struct.* **2019**, *212*, 552.
- [131] P. Bettini, G. Alitta, G. Sala, L. Di Landro, *J. Mater. Eng. Perform.* **2017**, *26*, 843.
- [132] O. A. González-Estrada, A. Pertuz, J. Quiroga, *Key Eng. Mater.* **2018**, *774*, 161.
- [133] Y. Nakagawa, K. Mori, T. Maeno, *Int. J. Adv. Manuf. Technol.* **2017**, *91*, 2811.
- [134] H. Mei, Z. Ali, I. Ali, L. Cheng, *Adv. Compos. Hybrid Mater.* **2019**, *2*, 312.
- [135] K. Ishii, A. Todoroki, Y. Mizutani, Y. Suzuki, Y. Koga, R. Matsuzaki, M. Ueda, Y. Hirano, *Adv. Compos. Mater.* **2019**, *28*, 383.
- [136] Q. Ding, X. Li, D. Zhang, G. Zhao, Z. Sun, *J. Appl. Polym. Sci.* **2020**, *137*, 48786.
- [137] E. A. Papon, A. Haque, *Addit. Manuf.* **2019**, *26*, 41.
- [138] Q. Li, W. Zhao, Y. Li, W. Yang, G. Wang, *Polymers* **2019**, *11*, 421.
- [139] A. A. Stepashkin, D. I. Chukov, F. S. Senatov, A. I. Salimon, A. M. Korsunsky, S. D. Kaloshkin, *Compos. Sci. Technol.* **2018**, *164*, 319.
- [140] F. Bárnik, M. Vaško, M. Handrik, F. Dorčiak, J. Majko, *Transp. Res. Procedia* **2019**, *40*, 616.
- [141] G. Sodeifian, S. Ghaseminejad, A. A. Yousefi, *Results Phys.* **2019**, *12*, 205.
- [142] G. Liao, Z. Li, Y. Cheng, D. Xu, D. Zhu, S. Jiang, J. Guo, X. Chen, G. Xu, Y. Zhu, *Mater. Des.* **2018**, *139*, 283.
- [143] G. Postiglione, G. Natale, G. Griffini, M. Levi, S. Turri, *Composites, Part A* **2015**, *76*, 110.